UNIVERSITY OF OKLAHOMA

GRADUATE COLLEGE

CHARACTERIZATION OF 802.11AD UNDER VARIOUS CHANNEL CONDITIONS

A THESIS

SUBMITTED TO THE GRADUATE FACULTY

in partial fulfillment of the requirements for the

Degree of

MASTER OF SCIENCE

By

DERRICK WILLIS
Norman, Oklahoma
2020

Downloaded from SHAREOK. Persistent Handle URL: https://hdl.handle.net/11244/326682

CHARACTERIZATION OF 802.11AD UNDER VARIOUS CHANNEL CONDITIONS

A THESIS APPROVED FOR THE
SCHOOL OF ELECTRICAL AND COMPUTER ENGINEERING

BY THE COMMITTEE CONSISTING OF

Dr. Hazem H. Refai, Chair

Dr. Samuel Cheng

Dr. Choon Yik Tang

© Copyright by DERRICK WILLIS 2020
All Rights Reserved.

Dedication

In loving memory of my grandparents

Samuel Willis Sr. and Willie "Susie" Willis

Acknowledgements

I would like to thank my advisor, *Dr. Hazem H. Refai*, for taking me under his wing and crafting my journey here at the University of Oklahoma. His critical thinking awakened in me an intellectual curiosity that has grown under his guidance. He will forever have my gratitude in life.

I want to thank *Dr. Samuel Cheng* and *Dr. Choon Yik Tang* as esteemed members of my thesis committee. Working with them has made this life achievement that I had merely dreamt of a reality for me.

I must also acknowledge all my fellow students, professors, and staff at OU for the unwavering encouragement they provided, regardless of day or time.

Special thanks to Michelle Farabough for the editing of this thesis.

Table of Contents

Acknowledgments.....v

List of Tables vii

List of Figures viii

Abstract.....x

Chapter 1: Introduction.....1

Contributions.....3

Chapter 2: Background and Related Work.....5

IEEE 802.11ad Throughput and Beam Reliability.....5

Superheterodyne Reception and Channel Power.....8

Chapter 3: Experimental Setup.....9

Environments.....9

Hardware.....10

Chapter 4: Network Performance.....16

Throughput.....16

Channel Power.....34

Throughput vs Channel Power.....39

Discussion.....44

Chapter 5: Conclusion and Future Work.....46

Conclusion.....46

Future Work.....47

References …….....48

List of Tables

Table 1. Original settings of the Anritsu MS2760A.……14

Table 2. Adjusted settings of the Anritsu MS2760A…….……...14

Table 3. Device list and configuration……...…16

Table 4. The mean throughput of obstruction scenarios.……...31

Table 5. Coefficients of the linear model of 802.11ad Channel Power……...36

Table 6. Statistics of the linear model of 802.11ad Channel Power……36

Table 7. Dongle orientation true channel power and extrapolated points…….…….....39

Table 8. Router orientation true channel power and extrapolated points…….…….....39

Table 9. Statistics of Linear Models of 802.11ad Channel Power vs. Throughput……...40

List of Figures

Figure 1. Fresnel zone visualization.……6

Figure 2. Adaptive beamforming structure.……7

Figure 3. Superheterodyne reception process of spectrum analyzer……...8

Figure 4. Directional antenna location within router.……...10

Figure 5. Antenna footprint of router.……...……11

Figure 6. Degree of coverage for Wi-Fi dongle.……11

Figure 7. Peraso W120 detailed component diagram…….……12

Figure 8. Portable millimeter band spectrum analyzer……13

Figure 9. Anritsu MS2760A 60 GHz millimeter wave.…….…...15

Figure 10. Lab hallway environment. a) Data collection illustration. b) Data collection actual image……18

Figure 11. Comparison of throughput vs meter 0° LOS. a) Uplink transmission. b) Downlink transmission.……19

Figure 12. Bunker environment SISO data collection.……..…22

Figure 13. Comparison of throughput vs time SISO. a) Uplink transmission. b) Downlink transmission.……23

Figure 14. Bunker environment 360° transmission……..…25

Figure 15. Throughput vs Angle for 360°. a) Uplink transmission. b) Downlink transmission……26

Figure 16. Bunker environment NLOS transmission.…….……..……29

Figure 17. Comparison of throughput vs time NLOS. a) Uplink transmission. b) Downlink transmission……30

Figure 18. Comparison of lost packet percentage vs meter……..……33

Figure 19. IEEE 802.11ad channel power vs meter linear model of orientation and environment. a) Dongle bunker. b) Router bunker. c) Dongle outdoor. d) Router outdoor……38

Figure 20. IEEE 802.11ad throughput vs. channel power linear models of channel conditions: a) Router outdoor environment, b) Dongle bunker environment.……..……41

Abstract

The latest Wi-Fi standard, IEEE 802.11ad, offers the most open and uncongested radio spectrum for wireless communication on the market today. The standard's capacity has maximum utility in locations with dense network activity, such as apartment buildings, airports, and other heavily populated locations. Because the standard boasts the highest theoretical throughput of 7 Gbps for devices with native support, market adoption has largely relied on the enthusiasm of technology vanguards. To increase widespread interest, backward compatible Wi-Fi dongles were created to regenerate legacy devices.

Although the MG360° Wi-Fi dongle platform detailed in this thesis showed a loss of 5 Gbps in theoretical network performance compared to native support, it gains portability across devices. The return of investment on these actions predicts a market growth of 7.4 billion USD by the year 2024. This thesis evaluates 802.11ad network performance in terms of throughput, channel power, and their relationship in three different but typical environments.

All experiments were examined through adaptive beamforming to discover the optimal multipath for signal interference. A multiuser domain, which is alternative to the current tri-band configuration available on the market, was simulated for exclusive 802.11ad usage. Parameters—serving as the degree of transmission,—and environmental reflectivity offered insights about the influence of the signal-to-noise (SNR) ratio in Wi-Fi communications. A polynomial empirical model assessed channel power and its relationship with distance. Extrapolation extended the polynomial model to help further explore the channel power and throughput relationship under adaptive beamforming.

Chapter 1: Introduction

Cutting-edge Wi-Fi technology has always lagged in enterprise adoption. Manufacturers have competed to serve this market by designing Wi-Fi universal serial bus (USB) dongles that update legacy devices, which has served to increase equipment reuse while minimizing overhead costs. With USB 3.0, backward compatibility retrofits older laptops not natively assembled using the Wireless Gigabit (WiGig) or 802.11ad standard.

This thesis evaluates the effect of the 802.11ad standard on Wi-Fi dongles with their performance and features confined to a USB interface. Introduced to the IEEE 802.11 protocol in December 2012 [1], 802.11ad was made available to the commercial market in late 2016 as a fiber optic replacement. Commercial devices used in this thesis were equipped with a 1x1 spatial stream or phased array antenna. They have been employed by manufacturers to specifically work in conjunction with each other. At the time the research for this thesis was conducted, six ultra-wide 2.16 GHz channels were available in the unlicensed industrial, scientific, and medical (ISM) band, ranging from 57.24 GHz to 70.20 GHz [2].

Increased spectrum capacity grants networks the ability to offload heavy traffic from the 2.4 GHz and 5 GHz bands in tri-band configuration. This capacity has potential density for frequency reuse [3], as expressed by Eq. (1).

$$Frequency\ reuse\ factor = \frac{1}{N} \qquad \text{Eq. (1)}$$

where N is the number of cells to complete a set of available frequencies (i.e., cluster).
As part of the 802.11 protocol, WiGig shares the same Media Access Control (MAC) layer as all previous Wi-Fi standards. Although this feature enables session switching, WiGig is incompatible at the physical layer. 802.11ad is characterized as a 60 GHz millimeter wave

(5mm) that can navigate above congested lower frequency spectrum bands. Earlier attributes inherited from previous standards include Orthogonal Frequency Division Multiplexing (OFDM) and Single input, Single-Output (SISO).

802.11ad has four modes with different modulations at the physical layer: 1) Control, 2) Single Carrier (SC), 3) Low-Power Single Carrier, and 4) OFDM. Authors have explained [4] that OFDM mode was immediately obsolete because the format used closely spaced carrier signals that interfered with one another. Although orthogonal orientation neutralized mutual signal interference, the technology is not required with 802.11ad's ultra-wide channel width.

The equipment used for the experiments reported in this thesis were designed on the signal carrier mode at the physical layer and the Π/2 16-QAM (Quadrature Amplitude Modulation) scheme. To date, this is the only physical layer and modulation scheme for the USB interface, making it suitable for the commercial market. Although the Modulation Coding Scheme (MCS) is proprietary, it is anticipated to be positioned in the MCS10 - MCS12 range for single carrier mode due to 802.11ad chip specification. Salient new features include extremely short range, adaptive beamforming, and very high throughput (VTH). Radio wave short range is affected by free space path loss (FSPL) when transmitting though the oxygen absorption band. The decibel expression of FSPL is formulated by Eq. (2).

$$FSPL(dB) = 20\log_{10}(d) + 20\log_{10}(f) - 147.55 \qquad \text{Eq. (2)}$$

where *d* is the distance between antennas and *f* is the frequency in gigahertz. FSPL is detailed at 68 dB per meter at 60 GHz frequency.

Low distance is beneficial when applied to niche situations requiring the prevention of eavesdropping captured signals, like military and espionage communication. This thesis reports tests in different environments that demonstrate the short range of the wave form and the effect

of these surroundings. One scenario that was tested determined whether the presence of reflective material could extend transmission range, despite large attenuation of the radio wave. The ancillary factor to these experiments was the addition of beamforming as essential to the standard.

Hence, all throughput measurements were under the influence of adaptive beamforming, which has a bi-directional training sequence that contours the transmitting and receiving radio wave. A study examining path characteristics as line-of-sight (LOS) is discussed herein; non-line-of-sight propagation (NLOS) was also examined. Channel power was investigated within the changing environmental settings. Empirical data was modeled according to variable distance of quarter meter or meter from the transmitter. After collecting this information, a second model was explored with throughput and channel power for determining the relationship between parameters. Extrapolation was used on channel power to extend the range and align data points with throughput.

Contributions

1. It was shown that throughput is highly dependent on reflectivity of the environment when adaptive beamforming is involved, as multipath selection affects range and performance.
2. Experiments demonstrated that depending on the angle, non 0° LOS transmission results in the loss of hundreds of Mbps, especially for the most reflective environment with the highest number of available multipaths.
3. Deploying 802.11ad in a multiuser domain greatly hinders its performance due to the current SISO feature on the market. As SISO only enables sequential transmissions, throughput rate drops as the router cycles Wi-Fi communication with each user.

4. 802.11ad adaptive beamforming technology consistently performed better on downlink transmissions compared to multitasking with optimal signal strength selection and upload transmission.
5. Empirical models of channel signal power vs. throughput were disrupted with adaptive beamforming. The consistent selection of optimal signal path combined with a reflective environment was found to adversely influence the signal-to-noise (SNR) concept regarding distance between transmitting antennas.

The balance of this thesis is structured, as follows.

- Chapter 2 introduces 802.11ad standard features and signal reception techniques necessary for downmixing the 60 GHz signal to an intermediate frequency.
- Chapter 3 describes the environments used for research reported in the thesis, as well as the hardware setups necessary for finding the 60 GHz signal using a portable spectrum analyzer.
- Chapter 4 focuses on network performance of throughput and channel power and employs an empirical approach for describing the relationship between these two factors within a defined environment.
- Chapter 5 concludes the analysis of the experiments and suggests further research that would contribute to market adoption of the standard.

Chapter 2: Background and Related Work

IEEE 802.11ad Throughput and Beam Reliability

802.11ad has been sufficiently developed for insertion into the IEEE 802.11 protocol family. Unfortunately, standard use with USB interfaces remains widely undervalued within the commercial market. Such underappreciation could be since most studies that examine various WiGig characteristics are based on experimental testbeds or limited commercial off-the-shelf products (COTS) with WLAN cards. COTS physical rate characteristic and throughput experiments based on varied distance were performed in [5]. Physical rate was reported as 50% faster than throughput when experiments involved multiple access points (AP) communicating to a single station (STA).

Authors in [5] also found that an association could be established between the AP and STA for cases with variables positioned up to 27m in distance for 0° (LOS). Notably, a testbed approach does not incorporate a fully compliant 802.11ad standard with hybrid MAC layer or modulation scheme. Authors in [6] developed a proof-of-concept evaluation with a reconfigurable antenna array and analyzed throughput performance under human blockage. Findings indicate that directional beams have less propagation loss with objects in the room compared to direct transmission against the human body, which recorded 20dB [7].

Because a 60 GHz radio wave is easily blocked, the propagation can be beneficial to detecting objects in the room and exploiting environmental dynamics. Range was unintentionally extended through signal diffraction from objects in the Fresnel Zone [8]. The Fresnel Zone is defined as the confocal prolate ellipsoidal region around the LOS positioned between the transmitter and receiver of radio waves. Violating the Fresnel Zone can cause radio waves to arrive at the receiver at different times (i.e., out of phase) because of the diffraction influence.

Depending on the level of phase shift, radio waves can interfere with transmission in either a constructive or destructive manner. Figure 1 provides a visualization of the Fresnel Zone.

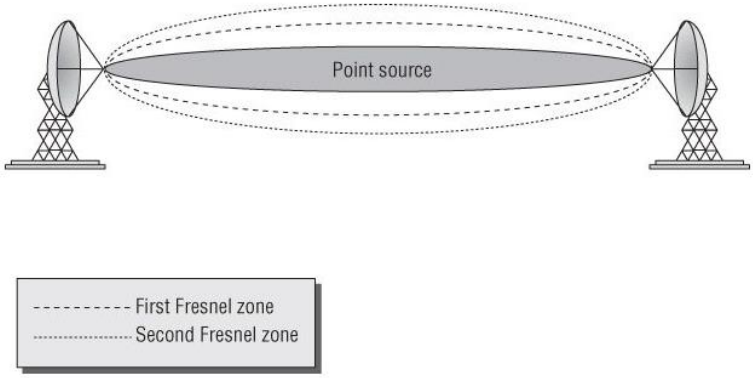


Figure 1. Fresnel zone visualization [9].

The application note indicates the critical nature of the first Fresnel Zone for successful point-to-point transmission. The widest point of the Fresnel Zone in these environments can be calculated by Eq. (3).

$$F_1 = 8.656 \times \sqrt{\frac{D[km]}{f[GHz]}} \qquad \text{Eq. (3)}$$

where F_1 is the maximum radius of the Fresnel Zone; D is the distance between the antennas; and f is frequency of the transmitted signal. If the objects block 60% or more of the first Fresnel Zone, destructive fading occurs.

An empirical analysis of this type of fading is given in [10], where path loss was modeled as a function of distance from the transmitter antenna. At the point of fading, impediments become tangent to the path of transmission; geometry was proven the primary factor of performance. An NLOS transmission with unfavorable propagation was attempted in [11], [12] and aimed at a solution of creating a link adaption algorithm. The objective was to

instantaneously predict the best multipath for mitigating link disconnects that lasted several hundred milliseconds before convergence.

The authors mentioned the lack of effective indicators for degraded beam reliability as the cause for downtime. Their proposal for triggering a beam search was collecting Packet-Error-Rate (PER) statistics from several packets given that reliability fell below the acceptable threshold. Adaptive beamforming has been proposed as a proactive solution for beam reliability. Authors in [13] demonstrated that during transmission, the radio wave's effective radiated power (ERP) by each antenna element can merge and overlay to enhance signal strength.

Constructive interference was used in desired directions, and destructive interference was found to lower signal strength in undesired directions for the transmitter. This behavior was repeated when acting as the receiver due to bidirectional control for a quality link connection. Figure 2 illustrates the general structure for adaptive beamforming.

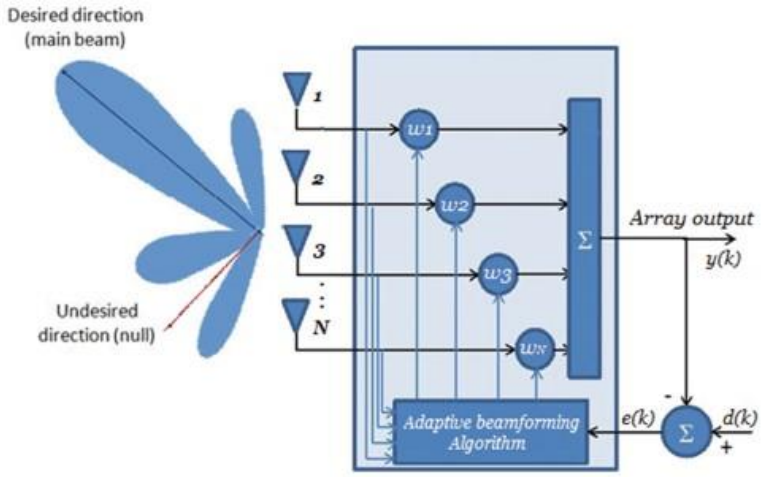


Figure 2. Adaptive beamforming structure [14].

In the figure, k is the number of narrow band user signals; y(k) is the beamformer output; d(k) is the desired signal; and e(k) is error used to control input weights of antenna elements through the algorithm.

IEEE 802.11ad Superheterodyne Reception and Channel Power

Adjustments were first made to the default settings of the spectrum analyzer to detect low level signals. Authors in [15] explained that Intermediate Frequency (IF) gain is part of a concept referred to as the Superheterodyne Reception. This technique downmixes the attenuated 60 GHz input signal with a low frequency signal generated by the local oscillator that is produced in the receiver. The result is a shifted intermediate frequency, which is the difference between original frequencies. The IF signal is then amplified with a 20dB gain and retains the same modulation of the original high frequency signal before final detection. Figure 3 shows the functional operation of the spectrum analyzer used in this thesis with IF gain activated.

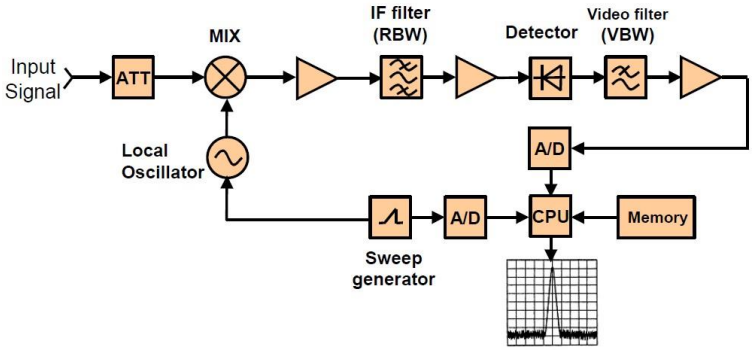


Figure 3. Superheterodyne reception process of spectrum analyzer [16].

Channel power is the signal power that is captured within the frequency range of the channel bandwidth [17]. For the 802.11ad standard, current measurements are accurate due to an uncongested frequency spectrum. While unwanted signals within the channel bandwidth can theoretically increase channel power, they lower efficiency [18]. Root mean square (RMS) detector is critical, as each sampled measurement point must be calculated in terms of a mean [19], primarily because channel power is calculated using an integrated bandwidth (IBW) on the signal power in the frequency range. Most signal power is contained in the main and side lobes of the signal, which results in a mean value with an absolute power unit of dBm.

Chapter 3: Experimental Setup

3.1 Environments

Multiple environments were used in my evaluation experimentation. The laboratory hallway on the fourth floor of Building 4 at the University of Oklahoma-Tulsa campus was used as the control group environment for testing Wi-Fi standard 802.11ad. Hallway surroundings are free from significant reflective material, although objects (e.g., metal storage cabinet, three metal doors, a windowpane, and metal railings of an exit ramp located between 1m and 2m) are positioned along the adjacent path of transmission. The hallway is 53m long and 4.2m wide.

The first environment for experimental grouping was a bunker location in Building 5 with a section that has been retrofitted to a Radio Frequency (RF) chamber for testing Wireless Local Area Network (WLAN) protocols. This location provides suitable accommodations for testing commercial, residential, and industrial devices. The chamber is 8.75m long and 3.28m wide with metal-lined observation windows for monitoring experiments in real time. The enclosure has four metal doors, a breaker box, an overhanging rail, and a side rail. There is a significant amount of reflective material along the radio wave transmission path.

The final experimental environment is and outdoor location outside the bunker. The open space is 13m long with operating space of 1.25m along the right side of the transmission path. A brick wall runs the length of the bunker, and a metal drainage system is positioned on the ground at around 5m to 6m of the transmission path. This testing area has the least amount of reflective material, although transmission can be influenced by environmental conditions (e.g., humidity on the 60 GHz signal).

3.2 Hardware

The Netgear Nighthawk XR700 [20] is a tri-band router suitable for 802.11ad and features a maximum transmission power (Tx) of 10 dBm. The router can broadcast a 60 GHz signal on WLAN channel 2 and channel 3 at the topmost throughput speed of 4.6 Gbps. There are six gigabit local area network (LAN) ports for wired connection to companion devices. For experiments reported in this thesis, the companion device was a laptop used for collecting and logging test results.

Four antennas are located on the back of the router and are allocated to the 2.4 GHz and 5 GHz ISM bands. Radio cards controlling the 2.4 GHz and 5 GHz antennas were disabled to prevent accidently testing the wrong Wi-Fi standard. The 802.11ad antenna was positioned at the router's front end, near the tip. Millimeter wave property limited the placement of the antenna due to high directionality of transmission. Figure 4 illustrates antenna placement inside the router.

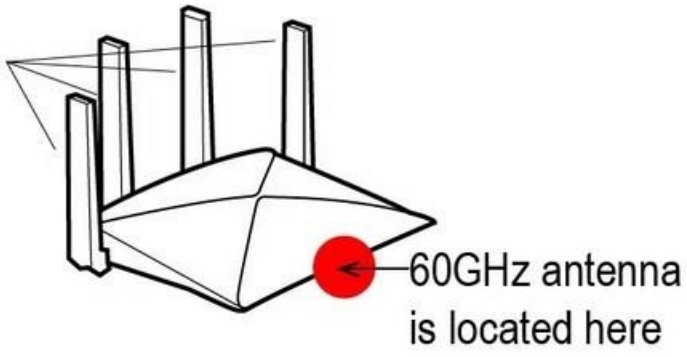


Figure 4. Directional antenna location within router [21].

The antenna is a 1x1 SISO with only one spatial stream for communication. According to manufacturer specifications, the maximum effective range of the XR700 router is 3m

horizontally, 1m vertically, and a 150° of semi-circle range. Figure 5 outlines the effective range for router operations.

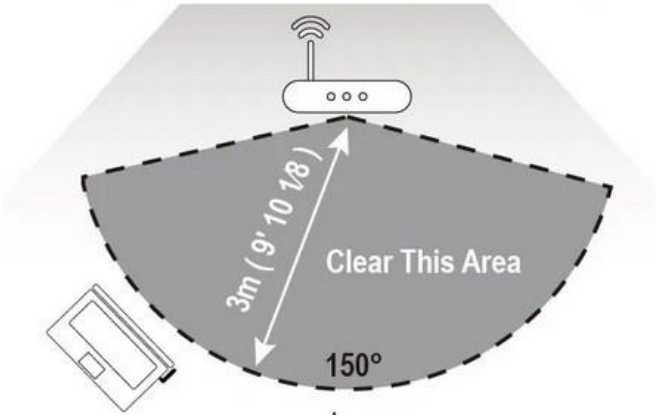


Figure 5. Antenna footprint of router [22].

An Atheros QCA9500 chipset for the Xr700 router was supplied by Qualcomm and enabled the 802.11ad standard. This chipset has been available in commercial routers since 2016. Since that time, several routers claimed superior performance in the residential market.

The Millitronic 360° USB Dongle [23] is 802.11ad certified and portable from laptop to laptop. The dongle is considered an essential companion to the XR700 for legacy devices (i.e., those not natively capable of 802.11ad transmission). While the dongle used for experiments reported in this thesis shares the same antenna footprint as earlier models, it boasts an extended range of 360° coverage—a significant improvement over the earlier 150° semi-circle range of the XR700 router (See Figure 6).



Figure 6. Degree of coverage for Wi-Fi dongle [24].

The USB dongle has a four-element antenna array that works together as a single antenna, leveraging a proprietary adaptive beamforming algorithm developed by Millitronic. The dongle can achieve a maximum throughput rate of 2 Gbps and operates only on default WLAN channel 2 for the 802.11ad standard. The W120 chipset was developed by Peraso and is shown in Figure 7.

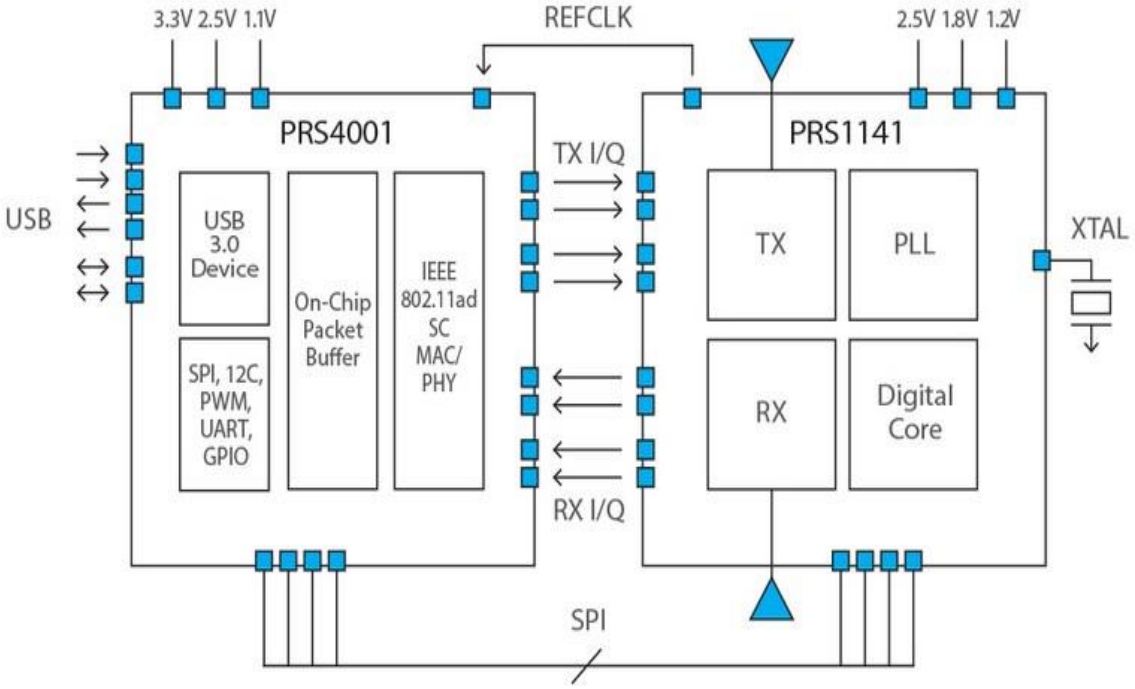


Figure 7. Peraso W120 detailed component diagram [25].

The Peraso dongle also has a 10 dBm Tx power limit and 6dB receiver power (Rx) noise figure. Three laptops—two legacy and one companion device for the XR700 router—were used in the experiments. An HP Spectre x360 served as the companion device and was connected via Ethernet wire to the Netgear XR700 router. The HP laptop archived all data for each throughput test and functioned as the server via the Iperf3 network performance measurement tool [26].

A ThinkPad T470s served as the primary legacy device (i.e., one not natively equipped to communicate with the 802.11ad Wi-Fi standard), as well as the platform for the attached MG360° USB dongle. The ThinkPad's WLAN card was disabled, allowing full control of radio wave testing through the USB dongle.

A Dell Precision 5540 laptop served as the second legacy device and was primarily deemed a substitute in the event of ThinkPad T470 hardware failure. Like the ThinkPad, the device was not manufactured with 802.11ad capability. A second MG360° USB dongle was attached to the Precision 5540, enabling it measure 802.11ad 1x1 SISO network performance (See Figure 13).

Anritsu MS2760A-0070 [27] is a portable spectrum analyzer used to detect and measure the 60 GHz frequency. A miniature 1.85 mm RF connector (V*) serves as a permanent fixture to the model. Attachments are configured as a precision waveguide for coaxing the dongle and standard gain horn antenna to guide the directional radio wave beam. Given these attachments, the model covered a frequency range of 9 kHz to 70 GHz. Figure 8 provides a rendering of the complete setup.



Figure 8. Portable millimeter band spectrum analyzer [28].

A Microsoft Surface Pro 4 with Windows 10 OS was connected via USB-C for screening Anritsu capture measurements. This device uses proprietary application software, namely Anritsu Spectrum Master, to detect when the analyzer is connected to a laptop. If used directly out of the box with default settings, the Anritsu cannot detect the 60 GHz signal and is characterized by a noise floor of -62 dBm. Table 1 details the original settings; Table 2details necessary adjustments for Anritsu.

Table 1. Original Settings of the Anritsu MS2760A

Setting	Adjustment
Resolution Bandwidth	3MHz
Video Bandwidth	3MHz
Amplitude Reference Level	0dBm
IF Gain	Off

Table 2. Adjusted Settings of the Anritsu MS2760A

Setting	Adjustment
Resolution Bandwidth	10KHz
Video Bandwidth	10KHz
Amplitude Reference Level	-10dBm
IF Gain	On

The first adjustment was implemented to reduce resolution bandwidth to 10 KHz with a goal of increasing spectrum frequency resolution, lowering average noise level, and enabling additional peaks for distinguishing low-strength signals. Video bandwidth is a time-domain low-pass filter equivalent to the mean for the frequency signal. This element was also altered to decrease displayed noise, rendering it equal to or less than the solution bandwidth.

Amplitude Reference level was changed to adjust the top grid line, which is the minimum signal level necessary to activate the intermediate frequency (IF Gain) setting.

Figure 9 demonstrates the resulting IF signal with an adjusted noise floor -88 dBm for regular high frequency signal detection. The figure shows a radio wave occupying the 60 GHz spectrum for WLAN channel 2.

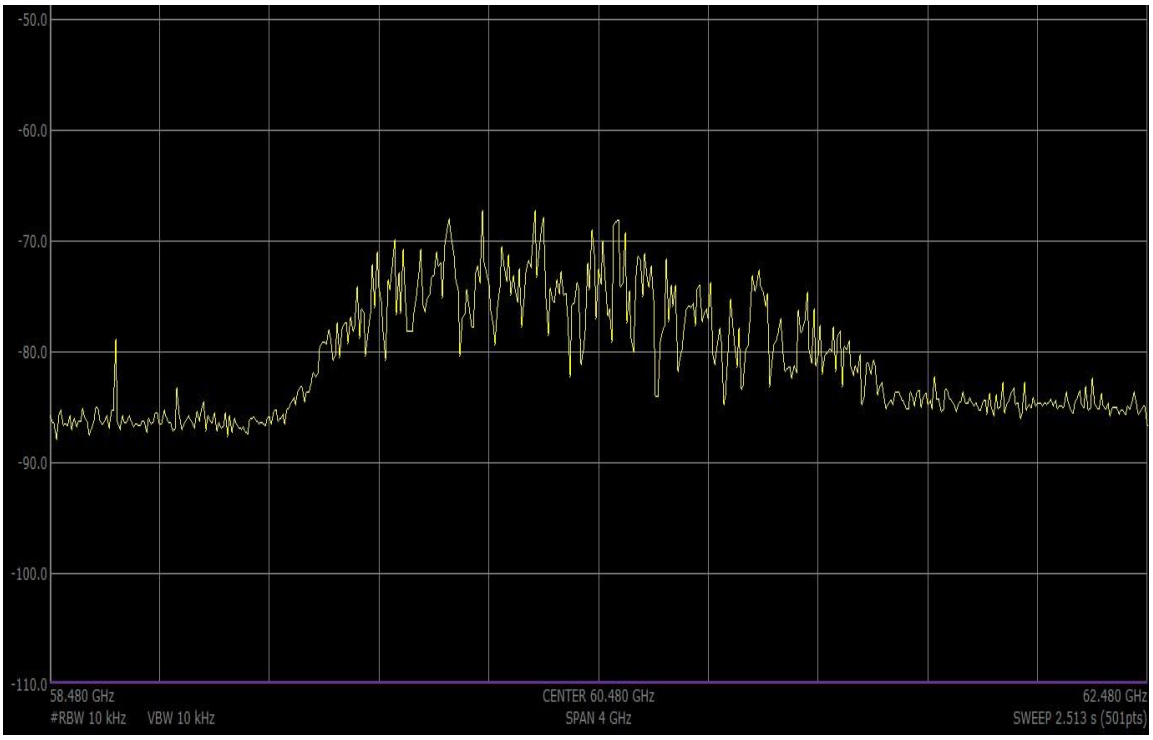


Figure 9. Anritsu MS2760A 60 GHz millimeter wave.

Chapter 4: Network Performance

4.1 Throughput

Several test setups were configured with the 802.11ad network broadcast by the router and the HP Spectre acting as the server. The ThinkPad T470s' MG360° dongle was attached to establish the client platform and complete the setup. The client and server laptop were not connected to the internet, effectively eliminating interference during throughput testing. The Anritsu ms2760A was connected to a Microsoft Surface Pro, which stored screenshots of channel power data.

Data collection was during nights and weekends. The physical presence of humans was also negated as a factor, as Windows batch files were used to automate throughput tests. Table 3 details the overall device configuration.

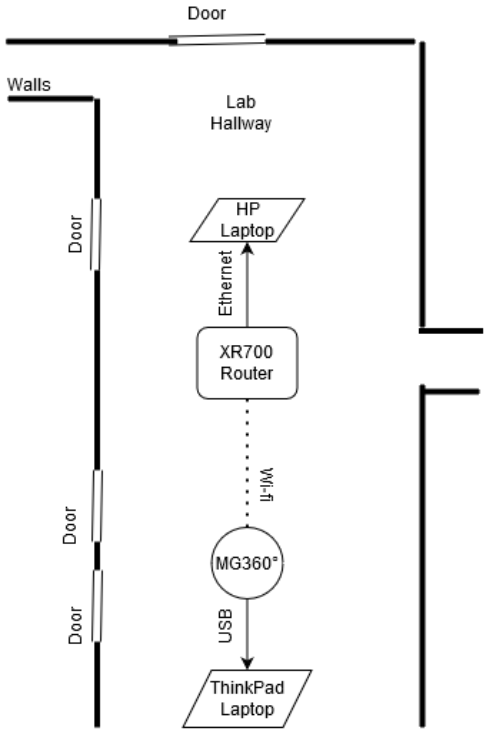
Table 3. Device List and Configuration

	Anritsu MS2706A	MG360° Dongle	ThinkPad T470s	HP Spectre X360	Netgear XR700	Microsoft Surface Pro 4
OS	Spectrum Master	Peraso	Windows	Windows	DumaOS	Windows
Version	V2019.9.1	2.7.171.344	10	10	V1.0.1.20	10
Network Interface	USB-C	USB 3.0	USB 3.0	Ethernet Cable	Ethernet Cable	USB-C
Iperf	-	-	3.1.3	3.1.3	-	-

The Iperf3 software tool was designed to generate network traffic across different Wi-Fi standards. The tool simulates Transmission Control Protocol (TCP) and User Datagram Protocol (UDP) real-world internet throughput, delay jitter, and rate of data loss performance. The TCP internet protocol served as the primary concentration for data analysis with bandwidth limits

disabled. UDP was also used to examine throughput lost packet rate in the lab hallway environment.

Zero-degree (0°) LOS throughput experiments were performed from router to client laptop for all three environments. These figures served as baseline performance for the throughput. Testing distance was changed in 1m increments until a maximum of 8m was reached between the transmitter and receiver (See Figures 10a and 10b).



(a)

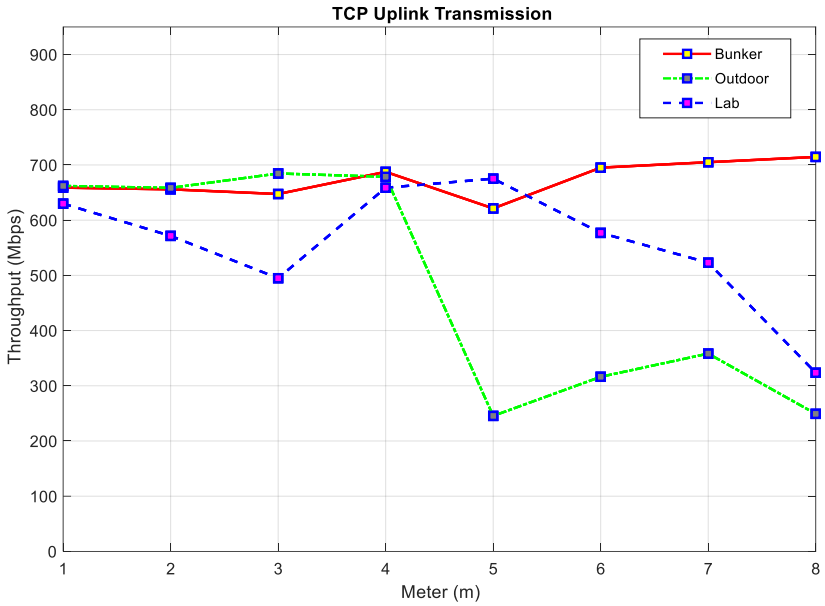


(b)

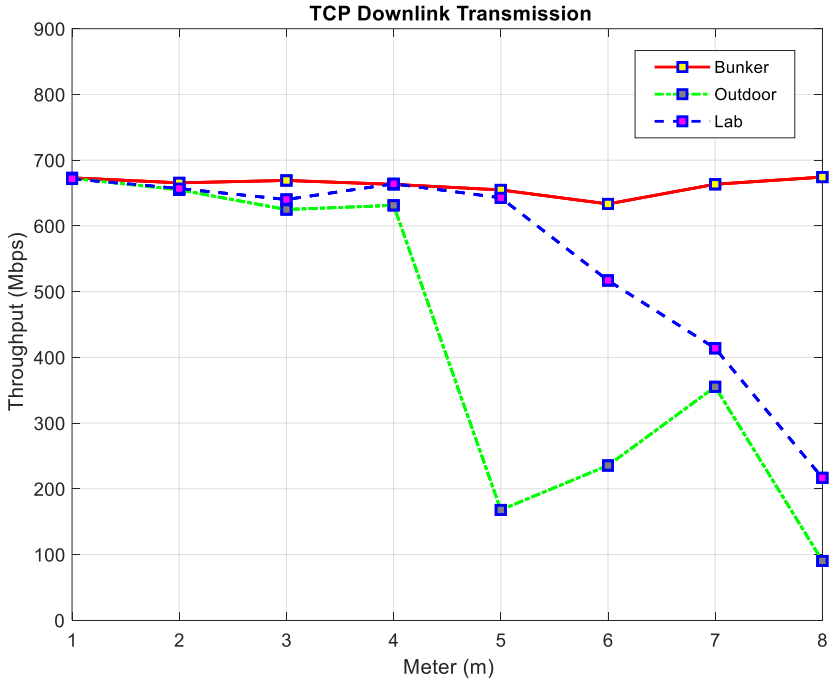
Figure 10. Lab hallway environment: a) data collection illustration, b) data collection actual image.

In the laboratory hallway, equipment was placed in the center to reduce the adjacent space of the transmission path from 4.2m to 2.1m. Ten throughput experiments were conducted per internet protocol at each meter increment for both uplink and downlink transmissions (i.e. 40 tests per meter for 60 seconds to obtain a total of 320 tests for 0° LOS transmissions so that mean and standard deviations could be calculated with confidence).

All equipment was configured to the default WLAN channel 2 with a center frequency of 60.48 GHz. Uplink and downlink transmission experiments were repeated 10 times, and mean was calculated for each environment. Before each test, a dummy test confirmed connection and time for exiting the area. All settings for the router and MG360° Wi-Fi dongle remained as the default. Results displayed in Figure 11a and Figure 11b were collected and analyzed using the test setup annotated in Figure 10.



(a)



(b)

Figure 11. Comparison of throughput vs. meter 0° LOS: a) uplink transmission, b) downlink transmission.

Figure 11a shows various throughput results for the uplink transmission of the MG360° Wi-Fi dongle in each environment when using the TCP protocol. The lab hallway was initially exhibited an uncharacteristic decline in throughput for the first 3m at 500 Mbps compared to its overall performance over 8m. It is possible that the metal guard rail positioned along the 2m– 3m section might trigger adaptive beamforming and lower throughput from destructive interference. Throughput recovered at 4m to nearly 650 Mbps—an increase of nearly 150 Mbps for only 1m. The highest mean for the lab hallway was achieved at 5m. This result suggested that the MG360° dongle adjusted signal strength via adaptive beamforming, not as a consequence of accurate decision-making. At 5m, throughput demonstrated expected logarithmical decay to near 300 Mbps.

The bunker showed consistent throughput performance when the distance increased between RF devices. Results could be affected by multipath influence on the MG360° dongle, as the environment has significant reflective material along the entire transmission path. Such multiple options allow a greater chance of selecting optimal beam path. Throughput rate averaged 700 Mbps or higher when analyzing the data for 6m or beyond. Notably, the studied environment simulates residential use of MG360° and shows far greater resiliency when operating above manufacturer specifications of 3m.

The outdoor environment had the highest trending throughput for the first 4m of uplink transmission before rapidly dropping to less than 300 Mbps at 5m. Because this environment had the least amount of multipath, the MG360° dongle could not compensate with constructive interference and increase signal strength. Only when distance was beyond 5m and MG360° had access to the metal rain drainage grate on the ground was signal strength able to increase. This outcome demonstrated how the device used low angle beamforming adaption for reflective

material. The only other reflective material in the environment was a brick wall adjacent to the transmission path. A throughput gap of 8m between the three environments proved to be an indication of expected results when considering reflective material for testing.

When analyzing downlink transmissions, Figure 11b demonstrated a more stabilized throughput decay of the lab environment. The 3m decline was not as pronounced, suggesting that the MG360° makes better decisions adjusting signal strength in the receiver role in certain environments. The signal remained level until 5m—the point at which decay began to affect performance. The decay curve was more pronounced at 6m, at nearly 500 Mbps, until it continued to decline to 200 Mbps. It is important to note that starting at 3m, the lab hallway signal transmission, occupied a middling performance compared to the other signals for the entire experiment.

The bunker signal maintained a high throughput rate mean for downlink transmission. In fact, it proved to be the highest mean throughput compared to the other environments in the experiment. Unlike the uplink bunker signal, downlink transmission did not trend over 700 Mbps, during uplink and downlink analyses, the bunker signal also had the least fluctuation of any signal.

Regarding the outdoor downlink transmission, throughput rate remained largely the same as the uplink until a more drastic decline in comparison occurred at 5m. At that point, the rate crossed the 200 Mbps threshold before making a recovery at 7m that resembled a linear increase. This increase nearly matched throughput rate of the lab environment at the same distance. It was observed that similar conditions were a factor when considering the drainage grate, which prevented flat piece-wise behavior of the throughput mean.

A Dell Precision 5540 was fitted with a second MG360° dongle for observing results of 1x1 SISO with multiple clients. A new client was connected to the router WLAN. The ThinkPad T470s, now user1, was placed -15° from 0° LOS away from the router using the unit circle as a reference. The Precision 5540, now user2, was placed 15° from 0° LOS. Both laptops were located 2m from the router and 1m from each other (See Figure 12).

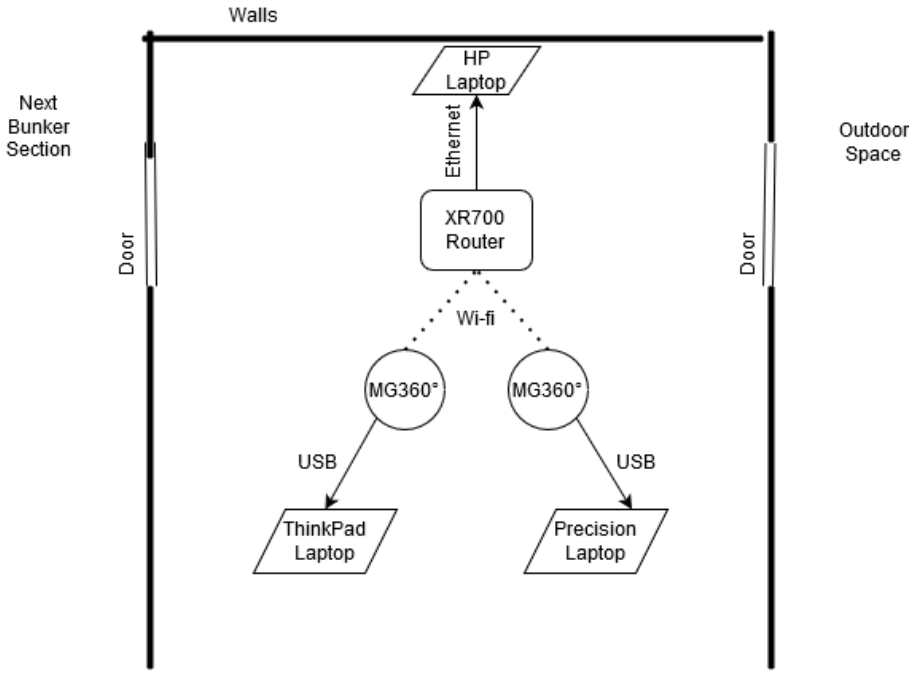
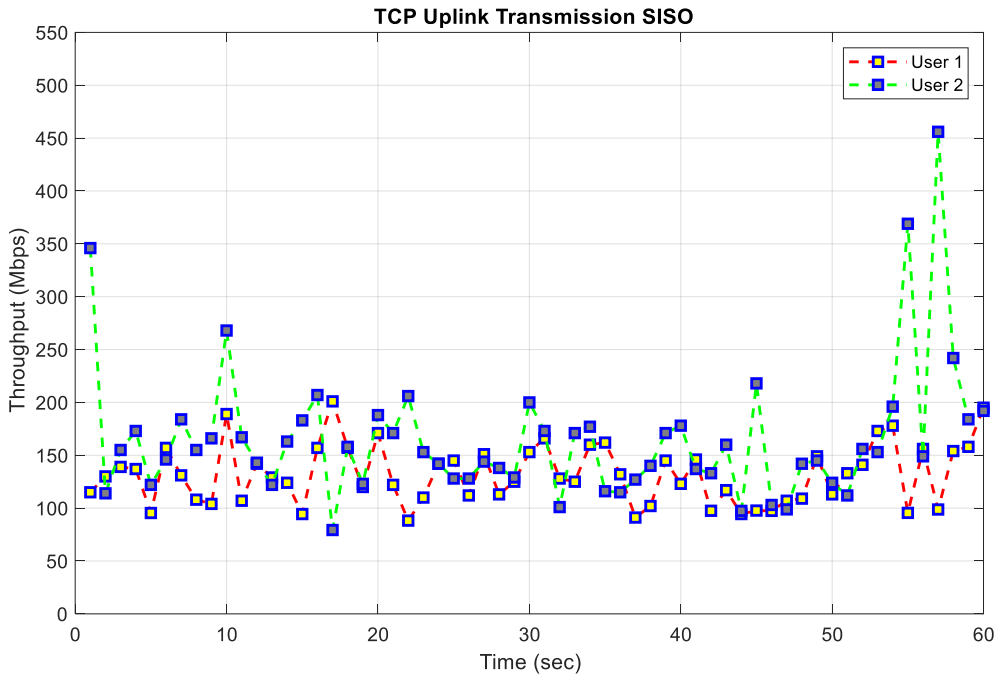
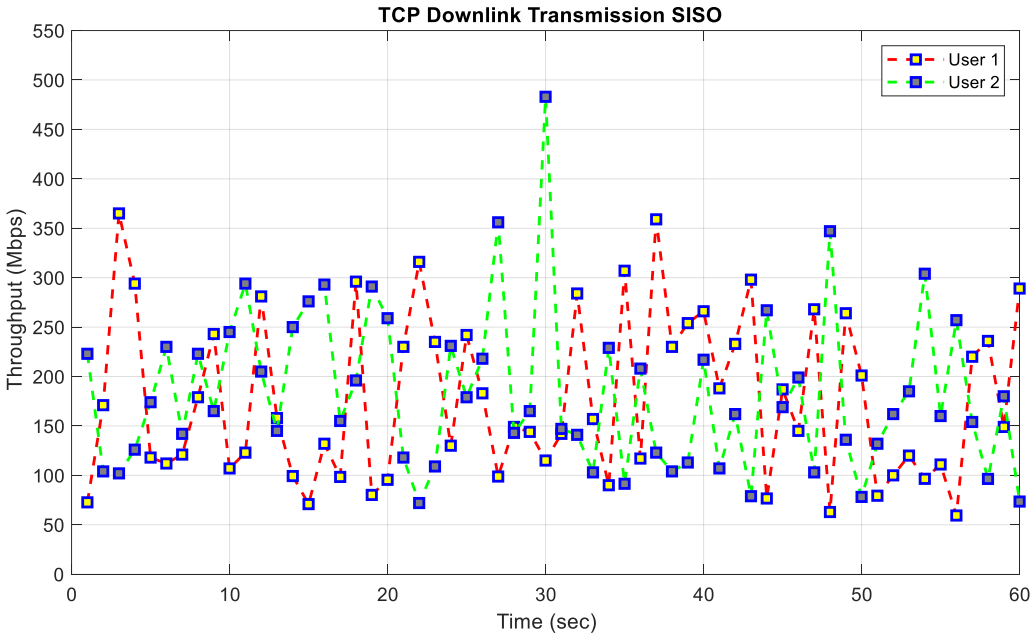


Figure 12. Bunker environment SISO data collection.

Testing for this setup was 60 seconds for uplink and downlink transmission. To explore additional throughput characteristics of the bunker environment, another client laptop was configured for two simultaneous transmissions to the STA antenna. This experiment had two AP adaptive beamforming algorithms competing for optimal link connections.



(a)



(b)

Figure 13. Comparison of throughput vs. time SISO; a) uplink transmission, b) downlink transmission.

After analyzing the results of SISO uplink transmissions in Figure 13a, there were two issues of concern. The first focused on SISO limitation, which can create congestion for multiple users. SISO technology accepts users on a first come, first serve basis. The problem was exacerbated in this study since the router had only one 802.11ad antenna. The network operated in a state of congestive collapse with the router antenna overloaded. Although Iperf does not give information about the lost packet rate in TCP mode, retransmission behavior may have contributed to the lowered throughput rate.

There were fewer than ten occurrences when 200 Mbps was achieved. Most throughput data ranged between 100 Mbps and 200 Mbps. Any point above this range was considered an outlier for the purpose of uplink analysis.

The second issue concerned adaptive beamforming consistently adjusting the signal via constructive or destructive interference. Default modulation for the MG360° rate control algorithm is 16-QAM. It is possible that due to channel conditions, rate control may have decreased to a simpler modulation. Also, it is important to note that the adaptive beamforming algorithm of the MG360° is proprietary and not open to the public. Thus, the impact of both features' corrective measures regarding congestive collapse of the network is unsure.

Analysis of downlink transmissions in Figure 13b suggests first-come first-serve throughput performance without congestive collapse. When both users shared the same spatial stream bandwidth, a seesaw pattern of user priority was discovered. Though this phenomenon occurred only a few times, users rarely kept priority for more than a few seconds of transmission. The range for most throughput performance for each user was approximately 50 to 350 Mbps. This result proved to be a lower throughput range compared to the uplink test with adaptive beamforming remaining a factor for signal strength manipulation.

Another throughput experiment performed only in the bunker environment mapped the angle to transmission at 15° increments. The router was situated in the corner on a 360° rotating platform with 0.5-meter distance from both walls. The client laptop was maintained at a 2m distance from the router with a 0.5-meter distance from the wall, as well, to simulate residential use (See Figure 14).

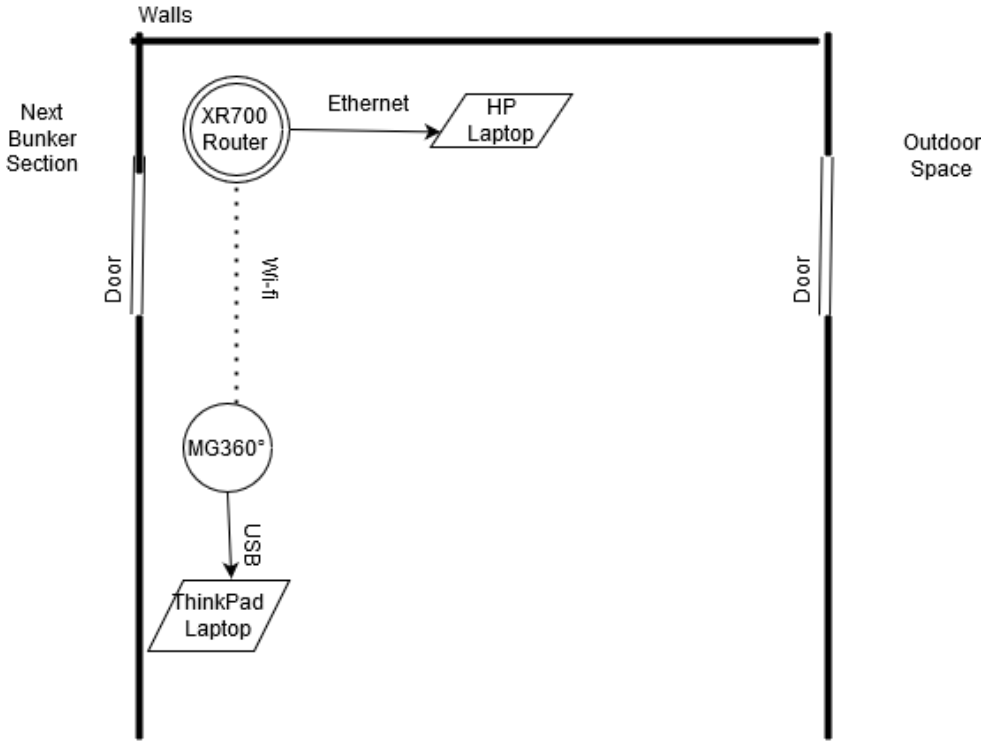
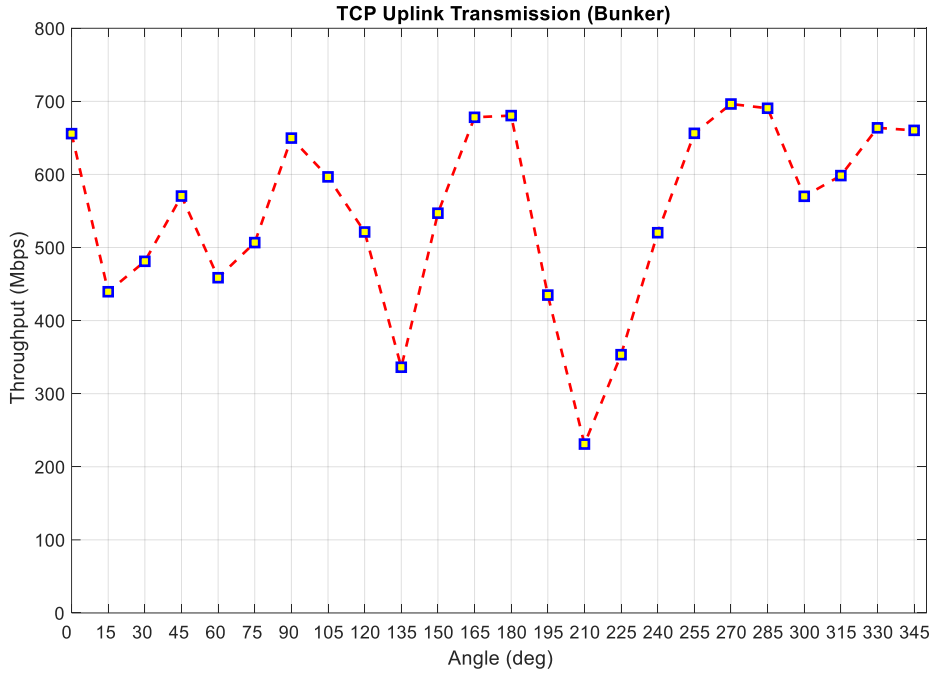
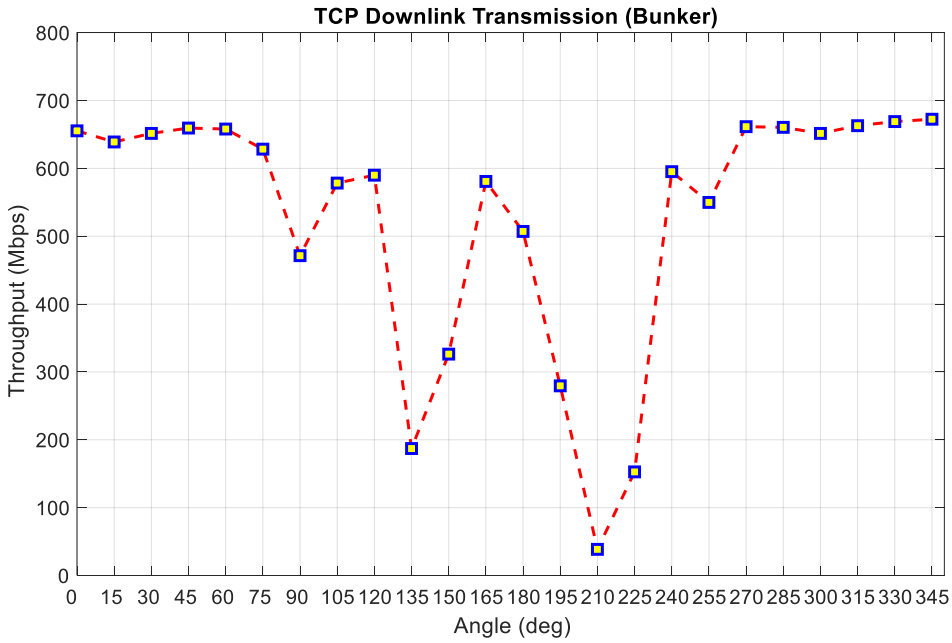


Figure 14. Bunker environment 360° data collection.

Operating procedure remained the same for 0° LOS regarding quantity and testing length for each communication protocol.



(a)



(b)

Figure 15. Throughput vs. angle for 360°: a) uplink transmission, b) downlink transmission.

The initial analysis indicated fluctuating throughput rate was sensitive to only 15° turns. Figure 15a shows TCP uplink transmission throughput instantly declined to 216 Mbps at the first 15° turn. As transmission incremented to 45°, MG360° dongle adjusted through multiple available multipaths, and increased throughput rate. The beamforming algorithm had difficulty locating the optimal signal path at certain angles, as throughput once again declined when reaching 60°. These observations indicated that uplink transmission experienced the optimal throughput rate when the router was not pointing toward certain diagonal positions in the testing environment. Even though the router antenna had the most space for transmission paths, its position made link connection difficult for the client laptop.

At 180°, the router was fully directed toward the back wall and away from the client laptop. Throughput performance unexpectedly increased. Given that 802.11ad beam directionality is standard, MG360° was expected to use NLOS propagation for a maximum throughput performance of nearly 700 Mbps. Two factors assisted in nullifying adaptive beamforming as throughput declined. First, the router was incrementally pointed toward the corner, which decreased the ability of radio wave signal power to bounce off more than one surface. Second, the client laptop lid self-shadowing became a factor between 180° and 210°, when it blocked the MG360° during testing. increments. Once self-shadowing cleared, the client laptop adjusted signal strength and increased throughput for increments from 225° to 270°. The laptop lid became an issue again for increments from 285° to 300°. Signal strength corrected thereafter.

Figure 15b shows that downlink transmissions were notably more stable against throughput declines when angle change first begins. Significant throughput decline did not occur

for 100+ Mbps until 90°; however, this behavior was contrary to results for uplink transmission, which increased at this angle. The pattern continued to decline, and throughput recovery angle changed until 120° was reached. When increasing from 120° to 135°, throughput experienced the single largest decline of the entire experiment for both uplink and downlink transmissions.

At this degree, the router was transmitting against the wall in a diagonal fashion. Fresnel Zone was violated any time the router was transmitting against the wall at a close distance. As the device rotated to 165°, it nearly returned to throughput rates attained at previous angles. From 120° to 240°, downlink transmission shared nearly the same performance profile, although downlink fell below 100 Mbps.

Earlier stated issues (e.g., router orientation facing the corner and client laptop self-shadowing) influenced performance profile. From 225° to 240°, throughput experienced the greatest increase in recovery due to a change in degree. When combined with earlier decreases, this result suggested that throughput fluctuations were higher for downlink transmission when encountering signal reflection and scattering. Since the router does not have adaptive beamforming, link connection must be managed via the bidirectional MG360° dongle.

When router rotated past 255°—at which point a small throughput decline was displayed, maximum throughput at 270° was attained. Throughput stability, originally displayed at the beginning of transmission, returned at 270° and remained at the same level until the experiment concluded. Uplink transmissions were found to be more sensitive to degree changes with smaller throughput fluctuation. Downlink transmissions had greater throughput stability when slightly off-angle from 0° LOS. Fluctuation were worse when transmissions encountered signal scattering and reflection.

The 802.11ad standard was also tested for baseline, blockage, and NLOS propagation during the final throughput test in the bunker environment. A blockage experiment was designed with transmitter and receiver distanced 2m apart with a human body positioned in the middle of the 0° LOS transmission. The second observation placed the router in the next bunker section with 1m longitude and 1m latitude for a total distance of 2m in the 90° arc (See Figure 16).

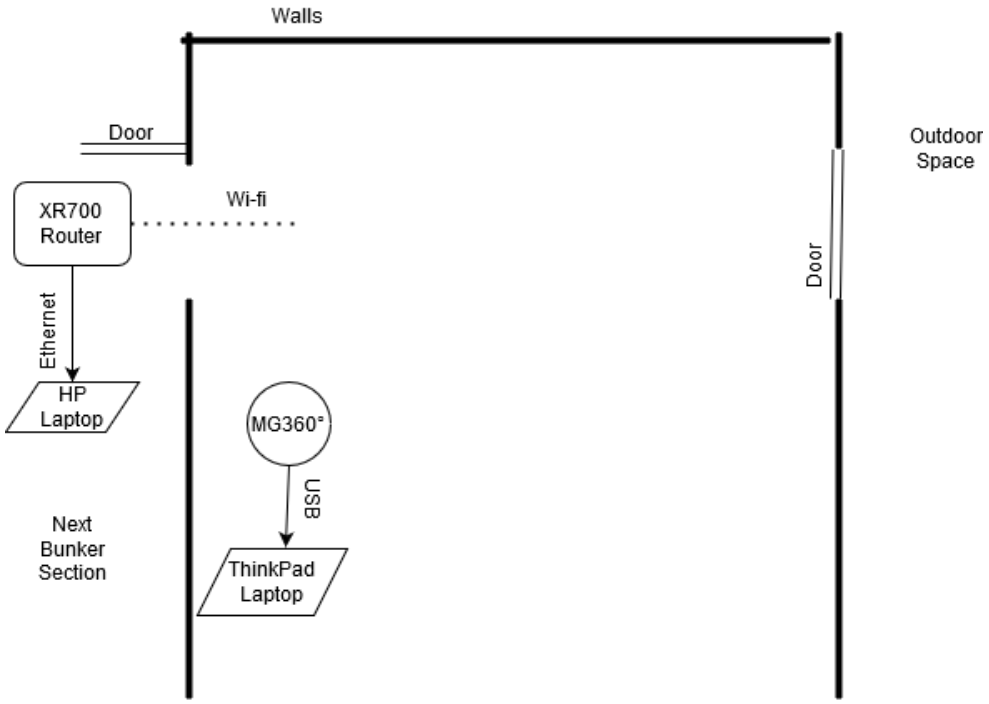
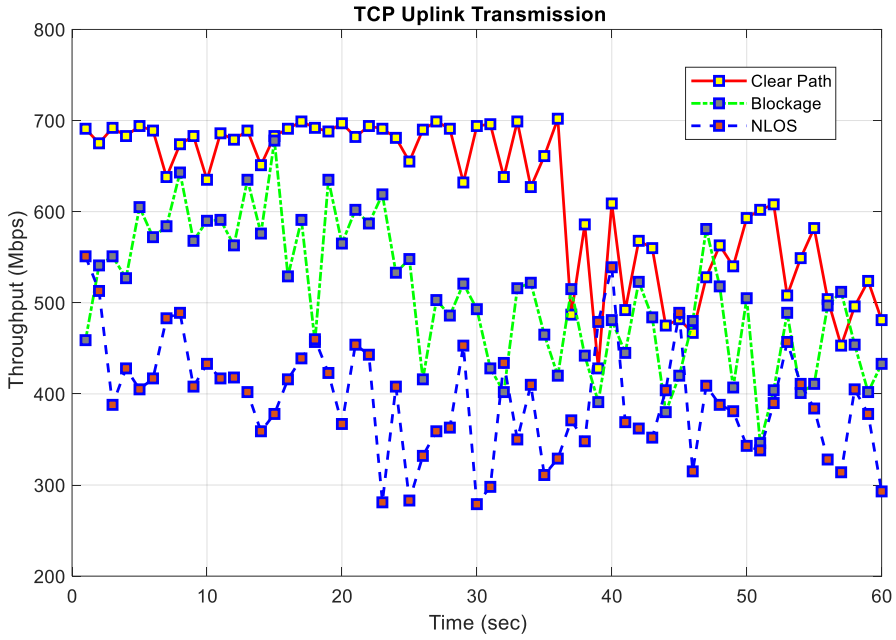
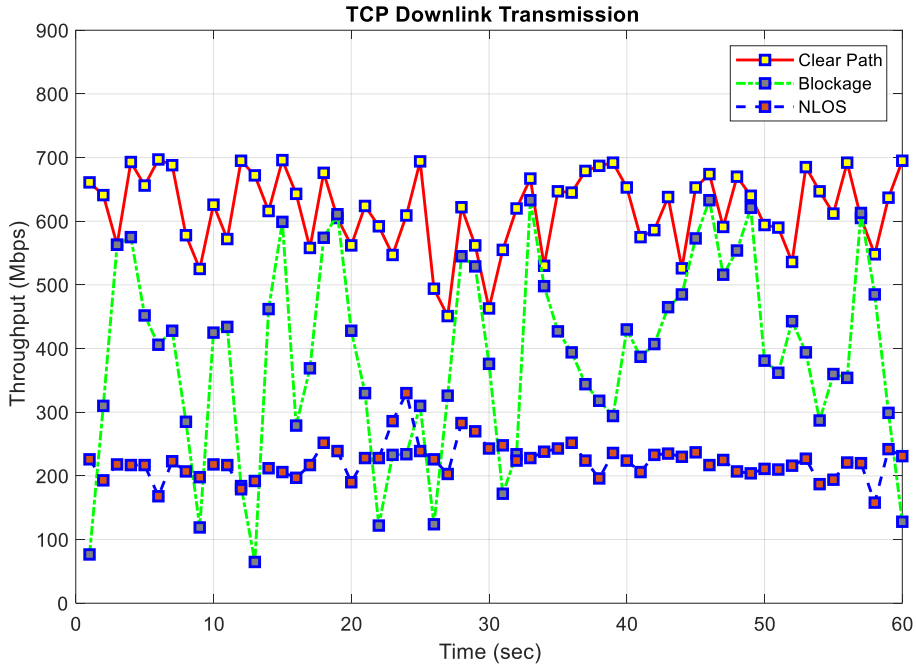


Figure 16. Bunker environment NLOS data collection.

A wall prevented the devices from achieving direct LOS. Once again, no one was present during automated testing.



(a)



(b)

Figure 17. Comparison of throughput vs. time NLOS: a) uplink transmission, b) downlink transmission.

Table 4. Mean Throughput of Obstruction Scenarios

Transmission	Clear Path (Mbps)	Blockage (Mbps)	NLOS (Mbps)
Uplink	618.77	507.37	393.8
Downlink	617.5	387.74	222.4

The objective was testing the influence of obstructions over a period of 60 seconds. The clear path scenario shown in Figure 17a demonstrates that uplink transmissions started at maximum throughput and remained there for the first 37 seconds with minimal variance before dropping below 600 Mbps. Because no one was physically present during this scenario, we can surmise that the MG360° device used destructive interference to lower signal strength. It is unclear whether lost packet threshold was reached or if another error occurred in the adaptive beamforming algorithm.

The blockage uplink transmission scenario indicated in Figure 17a shared the same test setup as the clear path experiment, except for the fact that one human body stood still directly in the 0° LOS transmission path during the entire test. Since millimeter waves cannot pass through objects, performance was measured for multipaths travelling around the human body. After beginning with a 4 second adjustment period, throughput dropped at approximately 25 seconds to 200 Mbps. Performance never recovered to the initial optimal data rate. In fact, results were nearly indistinguishable from the clear path transmission throughput performance.

The NLOS experiment for the throughput rate reported in Figure 17a shows variance in scale from small to large for the entire duration of the test. Large scale variance changes were throughput declines of more than 200 Mbps that occurred three times and were considered outliers. These throughput drops were timestamped at 22, 29, and 46 seconds. Overall performance was thought to be dependent on MG360° dongle multitasking to assume the transmission role and adjust signal strength each second.

Figure 17b displays the clear path downlink transmission performance as having an almost consistent throughput variance of medium scale (e.g., under 200 Mbps). The only exception was a large-scale throughput decline of exactly 200 Mbps at 25 seconds. Despite the consistent performance of downlink compared to uplink transmission, Table 4 shows that the two were virtually identical with regard to testing results. This can be explained by the fact that the uplink transmission peak performance was approximately 700 Mbps, which offset the decline to lower than 600 Mbps levels.

The blockage scenario shown in Figure 17b demonstrates significant throughput variance at the beginning of the test. This trend continued until 33 seconds had passed, when small incremental changes began to occur each second and produced a larger throughput variance shift. Because the router acted as transmitter, performance of the MG360° adaptive beamforming algorithm was interpreted as receiver and maintained a bidirectional link connection. This exchange in transmitter and receiver roles constituted a 23.6% decline for mean in performance, as demonstrated in Table 4.

The NLOS scenario shown in Figure 17b had the least amount of variance during both transmission throughput experiments. As receiver, MG360° easily located the optimal signal pathway, leveraging a 360° coverage of the room. This result also indicated that there was very little signal adjustment in link connection. In exchange for this stability, NLOS throughput mean also recorded a 43% decline in performance, as noted in Table 4.

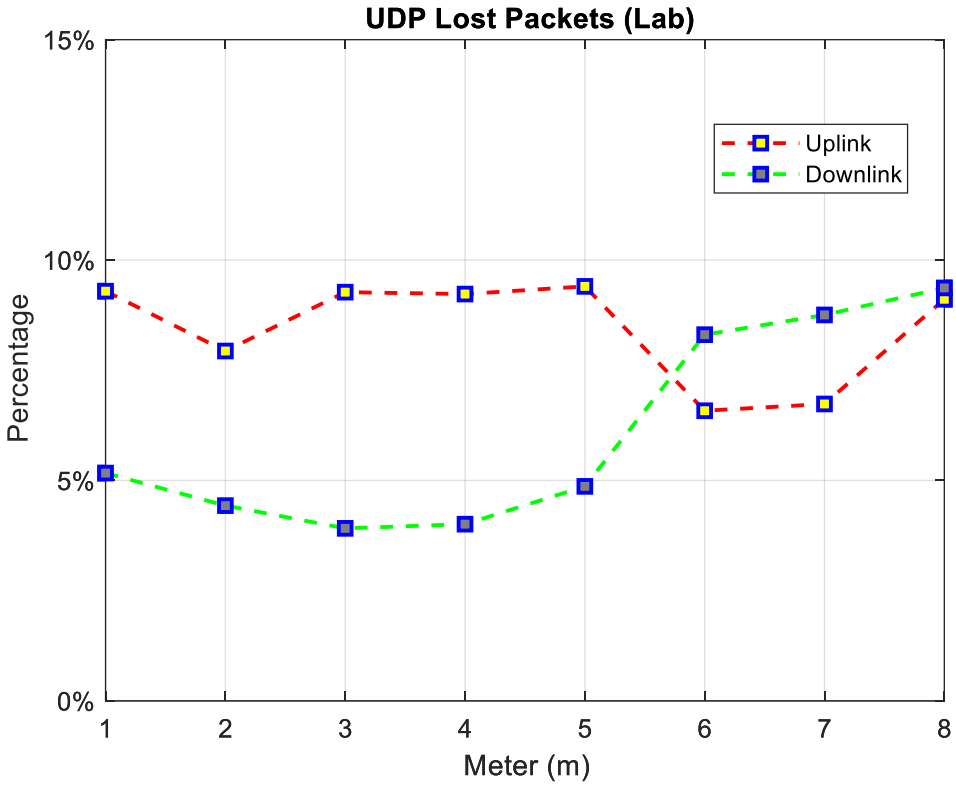


Figure 18. Comparison of lost packet percentage vs. meter.

To further expand on the lab hallway environment's throughput performance illustrated in Figure 11a, testing was executed in UDP mode to gather lost packet statistics in a set up identical to that reported in Figure 10. Results detailed that lost packet percentage did not exceed 10% for 8m in either uplink or downlink transmission in the lab environment. At 6m, there was a switching point where downlink transmissions experienced a greater percentage of lost packets. This trend continued until the end of the test, when both transmission protocols lost packets at nearly an identical rate. UDP is not as reliable as TCP, primarily because there are no acknowledgments for packet reception. This reality steers suspicion toward the adaptive beamforming algorithm for adjusted signal interference errors, as earlier theorized.

4.2 Channel Power

The test setup remained the same as throughput data collection when testing for channel power using the Anritsu in various environments (See Figure 10). Measurement mode options in the software activated the channel power feature. Iperf was set to continuous run mode without time limits. The device was aimed by hand, and the Anritsu collected channel power of the IF radio wave. Default setting was a sweep speed of 1.183 seconds, which is adequate despite changes to resolution and video bandwidths. The calculation for adjusting sweep speed is given by Eq. (4).

$$Sweep\ Time = k_{total} \times \frac{SPAN}{(RBW)^2} \qquad \text{Eq. (4)}$$

where k is the total amount of proportionality constant for SPAN/RBW; SPAN is the range of observed frequency; and RBW is the resolution bandwidth required for signals. IF channel power results were broken into orientation categories for analysis. The Iperf software tool generated indefinite network traffic using the TCP protocol for the experiments. When adjusted for millimeter waves, Anritsu sensitivity became a factor in data collection. For a digital spectrum analyzer, channel power is calculated by integrating FFT bins over the chosen channel bandwidth by Eq. (5).

$$y(x) = 10log_{10}\left(\left(\frac{B_s}{RBW}\right)\left(\frac{1}{x}\right)\sum_{i=1}^{x} 10^{\left(\frac{FFT(i)}{10}\right)}\right) \qquad \text{Eq. (5)}$$

where *y* is the data point of channel power in terms of dBm; B_s is the specified channel bandwidth; *RBW* is the resolution bandwidth; *N* is the number of data points in the frequency summation; and FFT is the current sample power of the bin *i* of the summation.

After increasing the distance between Anritsu device and transmitter, channel power eventually fell below the noise floor threshold. Transmitter and receiver maintained communication, although Anritsu was unable to detect IF channel power signal due to device sensitivity. A univariate polynomial is a sequence of terms, wherein every term is a coefficient multiplied with a monomial and every monomial is a power of variable x. A first degree polynomial was chosen to mathematically model the data and avoid overfitting via Eq. (6) with x given in units of meter.

$$\hat{y}(x) = P_1 x + P_2 \qquad \text{Eq. (6)}$$

Parameters P_1 and P_2 were approximated with 95% confidence intervals and are shown in Table 5. Goodness-of-fit parameters for the linear model are shown in Table 6. Intermediate frequency channel power models for device orientation and environments are based on Eq. (6) and shown in Figure 19. MATLAB was used to determine the statistics of the models with different channel conditions. Accuracy is determined according to the metrics of Sum Squared Error (SSE), Root Mean Square Error (RMSE), and R-Square. These parameters are incorporated into a goodness-of-fit test that evaluated the models.

SSE is the sum of squared estimate of errors or the sum of the squared residuals. In other words, the result is the deviation of the predicted values of the model fit line from the observed values of data and is given by Eq. (7).

$$SSE = \sum_{i=1}^{n} [y(x) - \hat{y}(x)]^2 \qquad \text{Eq. (7)}$$

RMSE is the root mean squared error and the standard deviation of the differences between predicted and observed data values. In practical use, this information reveals data concentration approximate to model fit line and is given by Eq. (8).

$$RMSE = \sqrt{\frac{\sum_{i=1}^{n}[y(x) - \hat{y}(x)]^2}{n}} \qquad \text{Eq. (8)}$$

R^2 is the coefficient of determination, which is the correlation between the predicted values and the observed values in a dataset, given by Eq. (9). For both SSE and RMSE lower values indicate better prediction performance of that model. This is in contrast of the R-Square metric which has a bounded value between 0 and 1. The closer the R-Square value trends toward 1 the more it indicates how well a model fits to the data for prediction. Factors such as multiple variables can lend toward increased unpredictability for the model and give a lower R-Squared value.

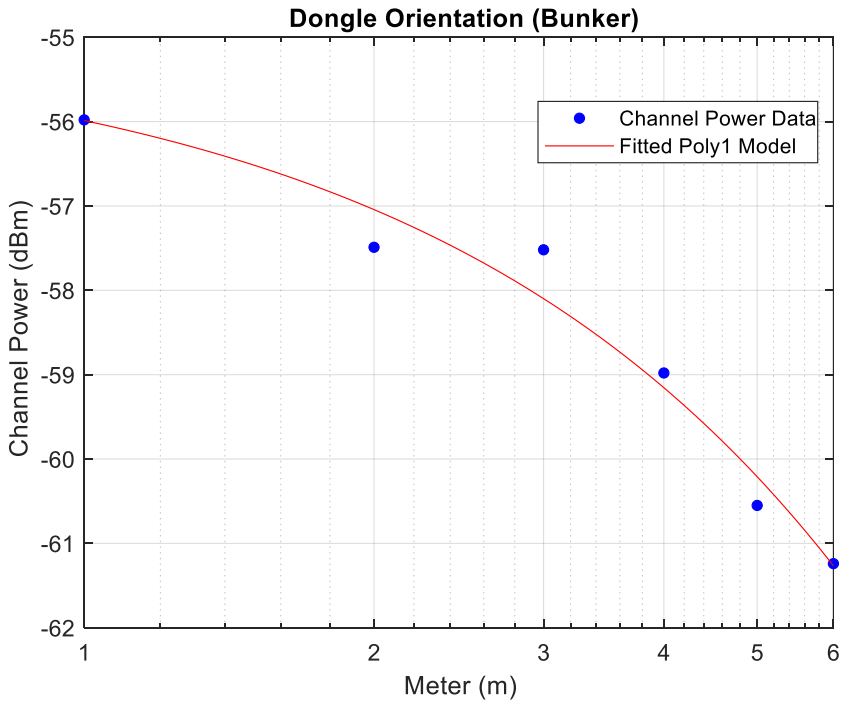
$$R^2 = 1 - \frac{SSE}{SST} \qquad \text{Eq. (9)}$$

Table 5. Coefficients of the Linear Model of 802.11ad Channel Power

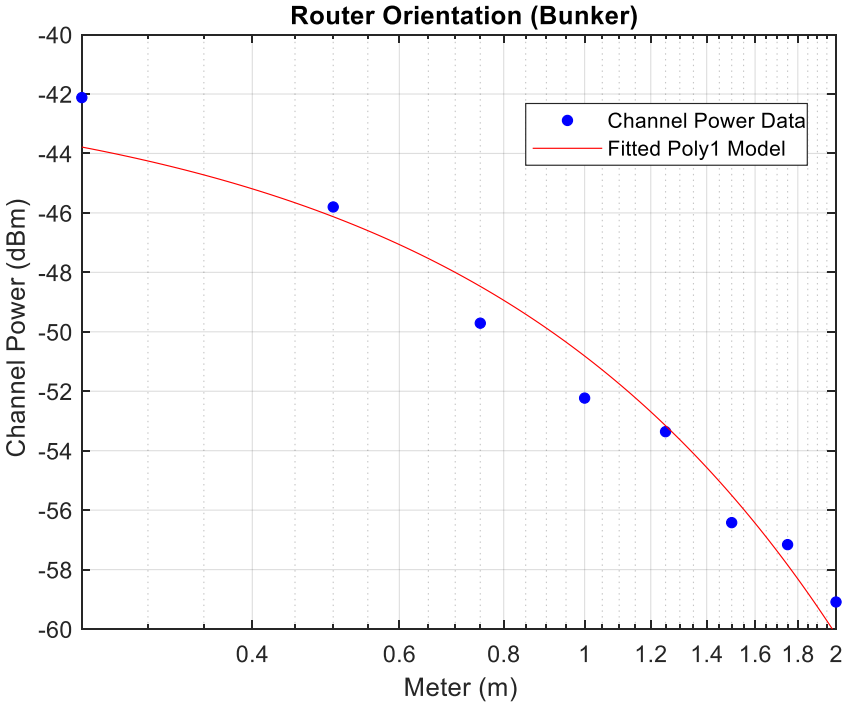
Orientation	P_1	95% Confidence Interval	P_2	95% Confidence Interval
Dongle (Bunker)	-1.055	[-1.329, -0.7815]	-54.93	[-56, -53.87]
Router (Bunker)	-9.374	[-11.22, -7.527]	-41.44	[-43.77, -39.11]
Dongle (Outdoor)	-10.52	[-13.16, -7.882]	-41.2	[-44.53, -37.87]
Router (Outdoor)	-3.798	[-4.028, -3.568]	-45.1	[-45.65, -44.54]

Table 6. Statistics of the Linear Model of 802.11ad Channel Power

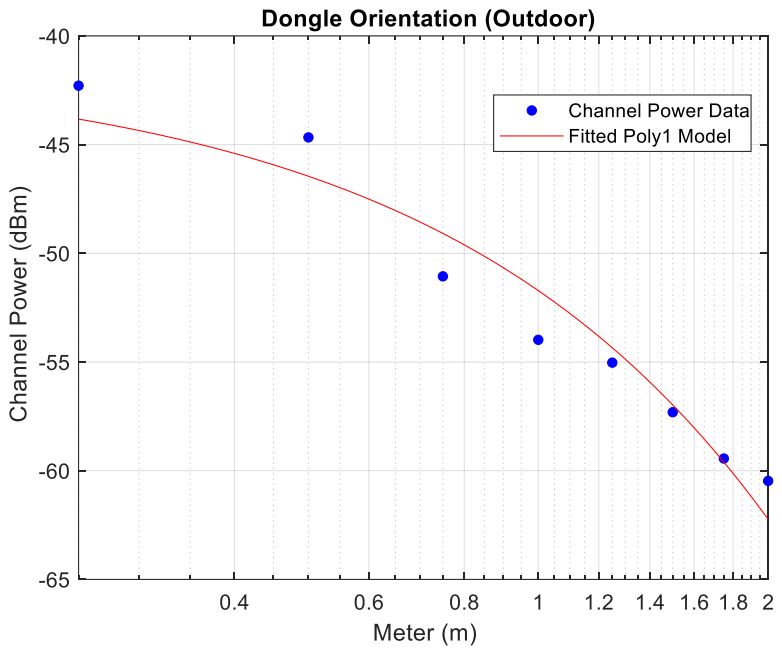
Orientation	SSE	RMSE	R-squared
Dongle (Bunker)	0.6814	0.4127	0.9662
Router (Bunker)	8.9753	1.2231	0.9625
Dongle (Outdoor)	18.2972	1.7463	0.9407
Router (Outdoor)	3.4225	0.4944	0.9890


Dongle Orientation (Bunker)
Channel Power Data
Fitted Poly1 Model
Channel Power (dBm)
Meter (m)
-55
-56
-57
-58
-59
-60
-61
-62
1
2
3
4
5
6

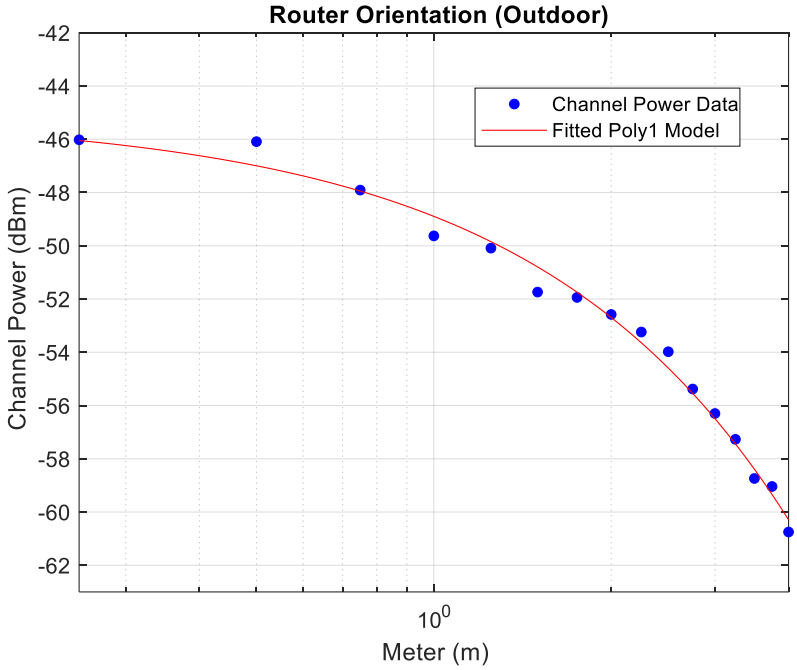
(a)


Router Orientation (Bunker)
Channel Power Data
Fitted Poly1 Model
Channel Power (dBm)
Meter (m)
-40
-42
-44
-46
-48
-50
-52
-54
-56
-58
-60
0.4
0.6
0.8
1
1.2
1.4
1.6
1.8
2

(b)



(c)



(d)

Figure 19. IEEE 802.11ad channel power vs. meter linear model of orientation and environment: a) Dongle bunker, b) Router bunker, c) Dongle outdoor, d) Router outdoor.

4.3 Channel Power vs Throughput

Empirical models were explored to determine the relationship between channel power and throughput performance in various channel conditions. The expected result is that higher channel power produces greater throughput performance. Since the IF millimeter wave could not be detected after channel power measurements reached the noise floor, extrapolation was employed to provide additional points to facilitate the development of empirical model. Extrapolation is the approximation of values, beyond the original observation range, from trends observed in known data obtained during measurement. Linear extrapolation can be calculated by Eq. (10) with *x* remaining in units of meters. This equation was used with MATLAB software.

$$E(x) = y(1) + \frac{x - x(1)}{x(2) - x(1)} \times [y(2) - y(1)] \qquad \text{Eq. (10)}$$

Linear extrapolation extended the range of channel power data points to the full distance of 8m necessary to match throughput values. Table 7 shows that the dongle oriented outdoor environment transmissions needed more extrapolated points compared to the other environments, since the channel power rapidly dropped below the noise floor of the Anritsu. Table 8 displays that bunker environment transmissions had the leading number of extrapolated points for router orientation with outdoor environment transmissions now having the least.

Table 7. Dongle orientation true channel power and extrapolated points

Environment	Increment	True Data Range	Extrapolated Points
Lab hallway	1m	1m - 6m	7,8m
Bunker	1m	1m - 6m	7,8m
Outdoor	1m	1m - 2m	3,4,5,6,7,8m

Table 8. Router orientation true channel power and extrapolated points

Environment	Increment	True Data Range	Extrapolated Points
Lab hallway	1m	1m - 3m	4,5,6,7,8m
Bunker	1m	1m - 2m	3,4,5,6,7,8m

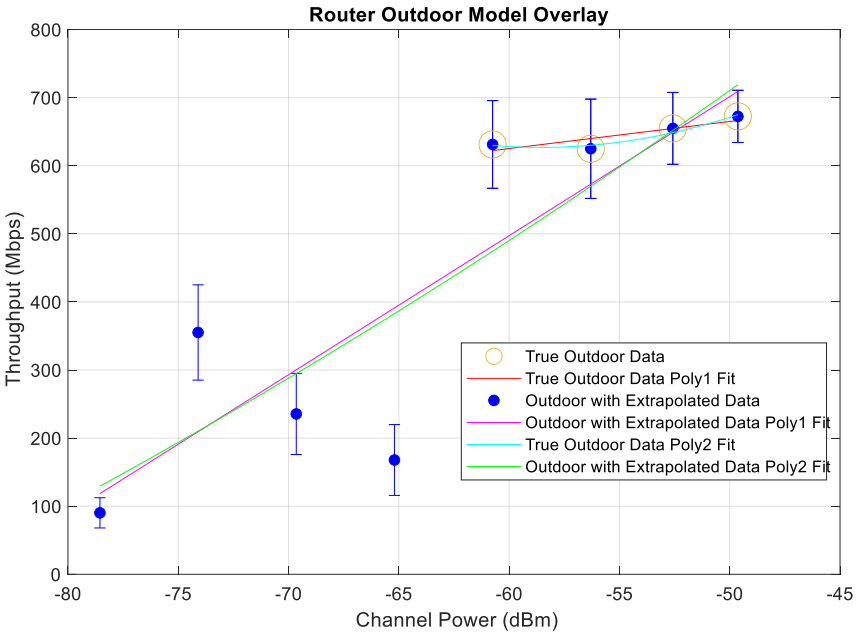
Outdoor	1m	1m - 4m	5,6,7,8m

The polynomial model used for channel power was maintained and increased to the second degree for results analysis. A second order polynomial given by Eq. (11) was used with real channel power results of Eq. (5) and extrapolated channel power of Eq. (10) as inputs to model the throughput-channel power relationship. Table 9 features goodness-of-fit statistics from MATLAB for various channel conditions using Eq. (7), Eq. (8), and Eq. (9).

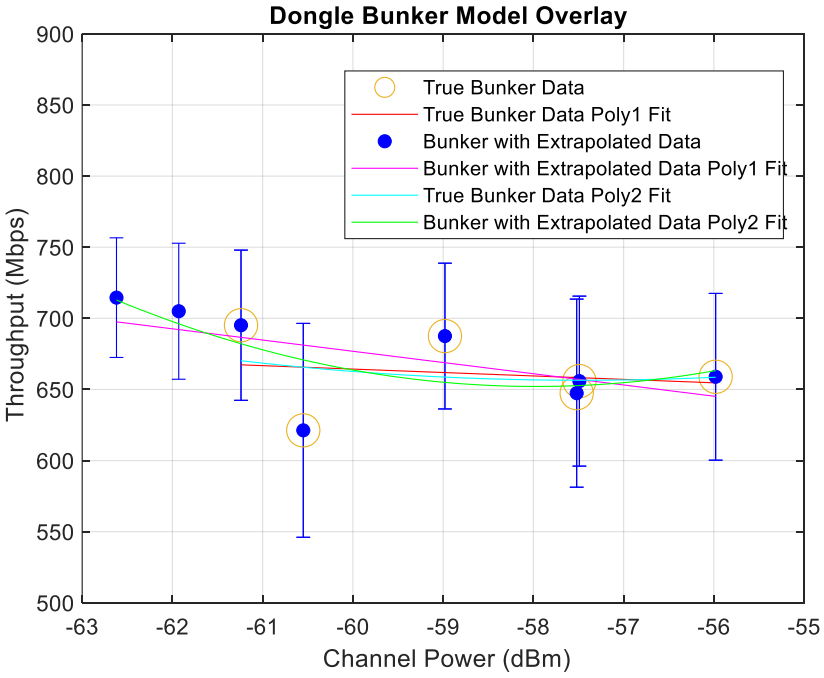
$$z(y(x)) = P_1(y(x))^2 + P_2(y(x)) + P_3 \qquad \text{Eq. (11)}$$

Table 9. Statistics of Linear Models of 802.11ad Channel Power vs. Throughput

Model	Transmission	SSE	RMSE	R-Square
Extrapolation 2nd degree polynomial model	Dongle (Lab)	41626	91.2430	0.5361
	Router (Lab)	5727.7	33.8458	0.9693
	Dongle (Bunker)	3821.6	27.6462	0.4748
	Router (Bunker)	713.3153	11.9442	0.4099
	Dongle (Outdoor)	26764	81.7985	0.8848
	Router (Outdoor)	35500	94.207	0.89
No Extrapolation 2nd degree polynomial model	Dongle (Lab)	21143	83.9500	0.1
	Router (Lab)	0	0	1
	Dongle (Bunker)	3507.6	34.19	0
	Router (Bunker)	Not enough data points for 2nd degree polynomial		
	Dongle (Outdoor)	Not enough data points for 2nd degree polynomial		
	Router (Outdoor)	75.4395	8.6856	0.9476
Extrapolation 1st degree polynomial model	Dongle (Lab)	64240	103.47	0.2841
	Router (Lab)	49113	90.47	0.7368
	Dongle (Bunker)	4761.1	28.1693	0.3457
	Router (Bunker)	1125.5	13.6959	0.0690
	Dongle (Outdoor)	86929	120.3669	0.7065
	Router (Outdoor)	102460	130.6776	0.7534
No Extrapolation 1st degree polynomial model	Dongle (Lab)	0	0.1	1
	Router (Lab)	0	0.1	1
	Dongle (Bunker)	3548.4	29.78	0
	Router (Bunker)	0	0	1
	Dongle (Outdoor)	0	0	1
	Router (Outdoor)	342.7184	13.09	0.76



(a)



(b)

Figure 20. IEEE 802.11ad throughput vs. channel power linear models of channel conditions: a) Router outdoor environment, b) Dongle bunker environment.

Figure 20 are sample overlays that visualize the relationship between observed values, extrapolated values, and the model fit lines that generate the statistics in Table 9. This Figure demonstrates the effect of the extrapolated points onto the developed models. Figure 20a contains the overlay of 4 different polynomial models that detail channel conditions for the router orientation. The 1st degree model fit line displayed for only true outdoor power measurements obtained within the first 4m has an SSE of 342.7184 as shown in Table 9. The 1st degree extrapolation version of this model contains the SSE of 102460 and includes the additional 4m for a total of 8m distance. The increase in SSE comes at the difference of 102117.28 or 29,796% which makes the model a highly inaccurate model in comparison from its observed metric-based model. Furthermore, RMSE shows a change from 13.09 to 130.6776. While this difference is also substantial at an 898% increase, it is not the highest swing in percentage for the metrics. The extrapolated version of the 1st degree polynomial is shown to be very detrimental to accuracy when extending the model to the full range of 8m. The 2nd degree best fit model of true outdoor data and its extrapolated version were also assessed with this channel condition. The 2nd degree true data model indicates an SSE of 75.4395 while the extrapolated version indicates the SSE of 35500. The SSE change is once again an abnormal increase of 46,957% when factoring the total 2nd degree extrapolated model. The RMSE for the higher degree models also follow the similar increase pattern of the lower degree polynomial models.

RMSE changes from 8.6856 to 94.207, a 984% rise, but not quite to the same elevated percentage levels of the SSE metric. The extrapolated versions of the polynomial models for this channel condition display a unilateral increase for all factors that significantly decreases its accuracy. When evaluating the two true outdoor data models together, it is observed that the 2nd

degree polynomial model has the lowest SSE number. The difference of SSE is the calculated number of 267.28 or a 78% decrease when upgrading from the 1st to 2nd model. The RMSE also drops to 8.6856 from 13.09 but is not as impactful in increasing the accuracy. The 2nd degree model is the superior choice when analyzing true outdoor data under this channel condition. More true data points (measurements) were obtained in the bunker, see Figure 20b. The 1st degree true bunker data mode with the dongle orientation has its SSE of 3548.4. On contrast, the 1st degree extrapolation model has SSE of 4761. As a result, the percentage increase is calculated as 34% only much smaller increase than outdoor extrapolated models. While the 1st degree extrapolated model did lower the accuracy, it did not show the significant accuracy loss demonstrated by the extrapolation models in Figure 20a. On the other hand, the RMSE shows an improvement in accuracy of 5.4%. Hence, the model accuracy loss due to extrapolation was lower by only 28.6%. The 2nd degree model obtained using bunker data is assessed with an SSE of 3507.6 which is lower than 3821.6 of the extrapolated version. A modest increase of 8.95% of SSE is the lowest calculated impact. The RMSE is once again lower for the extrapolated model at 27.6462 compared to 34.19 for the 2nd degree model. A 19.13% drop in RMSE shows that the extrapolated version is outperforming the real data model. The primary factor driving this is the influence of the channel conditions of a highly reflective signal environment. The R-Squared metric indicates that the data in this environment is highly unpredictable to model as well. The overall net accuracy favors the 2nd degree extrapolated model with 10.18%. The true bunker data model comparison between 1st and 2nd degree have very similar values of SSE, RMSE, and R-Square. The overall accuracy is higher with the 1st degree model by a net 13.66% with channel conditions.

Discussion

This section details the results of an experimental based study into the characteristics of IEEE 802.11ad. Throughput, channel power, and the relationship between them were explored relative to the impact of adaptive beamforming. The following conclusions were made.

1. Throughput performance for 0° LOS in different environments were analyzed under adaptive beamforming on a USB interface. The amount of reflective material present in the environment dictates the number of multipaths available for optimal radio wave transmission. In this study, the bunker environment had the most reflective material, and, thus, throughput hovered consistently around 700 Mbps even as the distance increased between transmitter-receiver antennas. This observation could also be seen in other testing environments, such as the lab hallway. The hallway had medium reflective material, and logarithmic decay was noticeable at 5m. The outdoor environment demonstrated throughput rate plummeting at 5m due to minimal reflective material.
2. When angle was introduced as a parameter in throughput experimentation there were profound effect on results, depending on type of radio wave transmission. Uplink transmissions were shown more volatile to even slight changes (e.g., 15°, which caused a 216 Mbps decline in throughput). Environments with highly reflective layouts were not robust enough to nullify volatility. Downlink transmissions were slightly more stable regarding degree adjustments, although results followed a comparable performance profile. Any off-center activity beyond 0° with the 802.11ad standard is discouraged based on evidence collected in this study.
3. SISO was examined with a second client device connected to the 802.11ad wireless network. As multiple clients were communicating sequentially, upload transmissions

caused congestive collapse. Only downlink transmissions showed true SISO activity (e.g., clients alternated greater and lesser throughput rates). This network characteristic is a hinderance to commercial and residential adoption, as it is financially prohibitive to require a 1:1 ratio of 802.11ad antennas to users for experimental throughput to approach a theoretical counterpart.

4. A mathematical approach was used to model channel power as a function of distance. A first degree polynomial was sufficient to characterize channel power according to device orientation and environment. Statistics, such as SSE, RMSE, and R-squared, gave numerical insight into model accuracy. One example evident in the bunker environment was that the dongle orientation of channel power measurement produced an SSE value of 0.6814. This compared with router device orientation of 8.9753 for an SSE, inferring greater deviation despite the same baseline environment.
5. The study found that equal parts of channel power and throughput were influential in a second degree polynomial model fit. Given external factors that affected either parameter, associated changes carried through into the model. In such situations where the model fit other scenarios, results did not provide useful information. Upon inspection, however, it was obvious that throughput was completely independent of channel power—a finding that is counter to industry consensus, as channel power has been described as merely the signal power of an active channel. The research detailed in this thesis explains that a highly reflective environment with adaptive beamforming can mitigate the influence of distance when determining the signal power arriving at the receiving antenna.

Chapter 5: Conclusion and Future Work

Conclusion

This thesis contains experimental results of the transmission control protocol for analyzing throughput parameters (e.g., LOS, environmental layout, and number of client devices on the IEEE 802.11ad network). Uplink and downlink transmission types were factored into results. As evidenced by performance profile of 0° LOS testing, environment became distinguished at 5m. Beyond this distance, the amount of reflective material determined in ascending order which environment had the greater throughput.

Another approach showed that angle of transmission caused volatile and lower throughput rates despite location in a highly reflective layout. The effect manifested with the surface's diagonal signal reflection when compared to a perpendicular impact that produced greater radio wave throughput. Device self-shadowing from a laptop lid blocked transmission and showcased 802.11ad vulnerability to a 60 GHz millimeter wave. This investigation also showed that multiple users on the 802.11ad network greatly hindered performance (e.g., congestive collapse occurs during either uplink transmission or sequential downlink communication between antennas).

The viability of the 802.11ad standard with SISO is weakened due to the feature's obsolescence with regard to new generation multiuser domains, even though the standard has throughput rates (e.g., up to 300 Mbps) that are comparable to the 802.11n standard when deployed with more than one user. One workaround is configuring the 802.11ad standard as a standalone emergency communication network coexisting with the 2.4 GHz and 5 GHz ISM bands. The channel power mathematical model in this work demonstrated low RMSE values across environments (i.e., from 0.4127 to a maximum of 1.7463).

The same polynomial model was increased to the second degree to discern the connection between channel power and throughput. Extrapolation of channel power for each environment resulted in extending data points to match throughput experimentation. The model resulted in higher-than-expected SSE deviations and a poorer fit, as indicated by RMSE. Statistical findings inspired underlying theory that both channel power and throughput relationships to SNR are indicators of goodness-of-fit between data and model.

Future Works

- Currently, 802.11ad commercial devices rely on the SISO 1:1 antenna system. An important consideration is how the standard would perform for network congestion in a multiuser domain if designed to at least have a single-input, multiple-output (SIMO) system.
- The 60 GHz frequency band is presently uncongested, due to the limited amount of active devices. It would be important to study throughput when co-channel interference is present via multiple 802.11ad devices. It would be helpful to know if signal-to-interference-plus-noise ratio (SINR) affect performance.
- The Millitronic MG360° Wi-Fi dongle uses a proprietary adaptive beamforming algorithm to determine optimal multipath. Given that another algorithm is used, users would benefit from knowing the effect on the influence of SNR for distance in certain reflective environments.
- Signal diffraction due to objects in the second Fresnel Zone can extend 802.11ad coverage. It remains unknown whether material composition matters more than the object orientation given a diffracting signal.

References

[1] Wireless Gigabit Alliance. [Online]. Available: http://www.wi-fi.org/discover-wi-fi/wigig-certified.

[2] Devopedia. 2020. "IEEE 802.11ad." Version 12, January 6. Accessed 2020-11-02. https://devopedia.org/ieee-802-11ad

[3] Rappaport, T. S. (2008). *Wireless communications: Principles and practice* (pp. 59). Upper Saddle River, NJ: Prentice Hall PTR.

[4] "WiGig: IEEE 802.11ad 60GHz Microwave Wi-Fi." (2020, November 5). Retrieved from www.electronics-notes.com/articles/connectivity/wifi-ieee-802-11/802-11ad-wigig-gigabit-microwave.php.

[5] T. Yamada, T. Nishio, M. Morikura and K. Yamamoto, "Experimental evaluation of IEEE 802.11ad millimeter-wave WLAN devices," *2015 21st Asia-Pacific Conference on Communications (APCC)*, Kyoto, 2015, pp. 278-282, doi: 10.1109/APCC.2015.7412525.

[6] Sur, S., Venkateswaran, V., Zhang, X., & Ramanathan, P. (2015). *60 GHz Indoor Networking through Flexible Beams: A Link-Level Profiling.* SIGMETRICS '15.

[7] Joshi, kishor chandra & Hersyandika, Rizqi & Prasad, Venkatesha. (2019). Association, Blockage, and Handoffs in IEEE 802.11ad-Based 60-GHz Picocells—A Closer Look. IEEE Systems Journal. PP. 1-10. 10.1109/JSYST.2019.2937568.

[8] Campbell Scientific. (2016). *Line of Sight Obstruction* (App. Note Code: 3RF-E). Retrieved from Campbell Scientific website: https://s.campbellsci.com/documents/us/technical-papers/line-of-sight-obstruction.pdf

[9] Pindoria, A. (n.d.). Fresnel Zone [Image]. Wordpress. https://dot11ap.wordpress.com/cwna/radio-frequency-rf-technologies/line-of-sight-and-fresnel-zone-issues/

[10] N. Moraitis and P. Constantinou, "Indoor Channel Measurements and Characterization at 60 GHz for Wireless Local Area Net-work Applications," *IEEE Transactions on Antennas and Propagation*, vol. 52, no. 12, pp. 3180–3189, 2004

[11] Sur, S., Pefkianakis, I., Zhang, X., & Kim, K. (2017). *WiFi-Assisted 60 GHz Wireless Networks. Proceedings of the 23rd Annual International Conference on Mobile Computing and Networking.*

[12] Sur, S., Zhang, X., Ramanathan, P., & Chandra, R. (2016). BeamSpy: Enabling Robust 60 GHz Links Under Blockage. *NSDI.*

[13] Naceur, Aounallah & Merahi, Bouziani. (2019). Initialization of LMS and CMA Adaptive Beamforming Algorithms with SMI for Smart Antenna System. 10.1007/978-3-319-97816-1_38.

[14] Naceur, Aounallah & Merahi, Bouziani. [Adaptive signal processing system]. (2019). Initialization of LMS and CMA Adaptive Beamforming Algorithms with SMI for Smart Antenna System. 10.1007/978-3-319-97816-1_38.

[15] "Superheterodyne Spectrum Analyzer: Sweep Spectrum Analyzer." (2020, November 7). Retrieved from https://www.electronics-notes.com/articles/test-methods/spectrum-analyzer/superheterodyne-sweep-swept-spectrum-analyser.php.

[16] Anritsu. (n.d.). Principals of a Spectrum Analyzer [Image]. Retrieved from https://www.naic.edu/~phil/hardware/Misc/anritsu/SpectrumAnalyzer_basis_of.pdf

[17] "Occupied Bandwidth and Channel Power Measurements with a Real-time Spectrum Analyzer." (2020, November 7). Retrieved from https://www.silvertoneelectronics.com/sites/default/files/documents/Occupied-Bandwidth-and-Channel-Power-Measurements-with-a-Real-time-Spectrum-Analyzer.pdf

[18] "5 RF Transmitter Measurements Every Engineer Should Know." NI, 23 July 2019, www.ni.com/en-us/innovations/white-papers/14/5-rf-transmitter-measurements-every-engineer-should-know.html.

[19] Sander, Kay-Uwe S. (2003). *Power Measurement on Pulsed Signals with Spectrum Analyzers* (App. Note Code: 1EF48_2E). Retrieved from Rohde & Schwarz website: https://cdn.rohde-schwarz.com/pws/dl_downloads/dl_application/application_notes/1ef48/1EF48_2E.pdf

[20] Nighthawk AD7200, Model XR700 Router, https://www.downloads.netgear.com/files/GDC/XR700/XR700_UM_EN.pdf

[21] Millitronic. (n.d.). [60 GHz antenna location]. Retrieved from https://millitronic.com.tw/mg360/

[22] Millitronic. (n.d.). [Netgear XR700 antenna footprint]. Retrieved from https://millitronic.com.tw/mg360/

[23] Millitronic MG360, USB 3.0 Dongle, https://fccid.io/2AJASU3WG360/User-Manual/User-Manual-4090885.pdf

[24] Millitronic. (n.d.). [MG360° antenna footprint]. Retrieved from https://millitronic.com.tw/mg360/

[25] Peraso. (n.d.). Peraso W120 Chipset [Image]. Retrieved from https://perasotech.com/w-series-products/

[26] Iperf. [Online]. Available: http://iperf.fr.

[27] Anritsu Spectrum Master MS2760A, Spectrum Analyzer, https://dl.cdn-anritsu.com/en-us/test-measurement/files/Manuals/Users-Guide/10580-00427K.pdf

[28] Anritsu. (n.d.). [Anritsu MS2760A with tripod]. Retrieved from https://dl.cdn-anritsu.com/en-us/test-measurement/files/Manuals/Users-Guide/10580-00427K.pdf